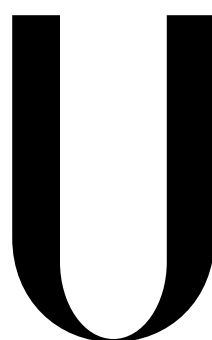


Universidade de Lisboa
Faculdade de Ciências
Departamento de Física



LISBOA

UNIVERSIDADE
DE LISBOA

**Human Brain Networks: An
Investigation on Cortical Thickness,
Resting-State fMRI and Structural
Connectivity as Assessed by
Tractography**

Ana Filipa Canha Figueira

DISSERTAÇÃO

MESTRADO INTEGRADO EM ENGENHARIA BIOMÉDICA E BIOFÍSICA
PERFIL EM RADIAÇÕES EM DIAGNÓSTICO E TERAPIA

2013

Universidade de Lisboa
Faculdade de Ciências
Departamento de Física



**Human Brain Networks: An
Investigation on Cortical Thickness,
Resting-State fMRI and Structural
Connectivity as Assessed by
Tractography**

Ana Filipa Canha Figueira

DISSERTAÇÃO

MESTRADO INTEGRADO EM ENGENHARIA BIOMÉDICA E BIOFÍSICA
PERFIL EM RADIAÇÕES EM DIAGNÓSTICO E TERAPIA

Orientador Externo: Doutor Chris Clark

Orientador Interno: Doutora Rita Nunes

2013

This thesis is dedicated to my parents.

Acknowledgements

This thesis would not have been possible without the help of many people at the Institute of Child Health, UCL, at the Faculty of Sciences of the University of Lisbon and at the Institute of Biophysics and Biomedical Engineering, to whom I would like to thank.

I would like to express special gratitude to my supervisors Dr Chris Clark and Dr. Rita Nunes for the useful comments, remarks and guidance through the learning process of this master thesis.

I would like to thank the PhD Students and post-doctoral research scientists of the Imaging and Biophysics department of the Institute of Child Health, UCL, for all their patience and time lost helping me in the course of this project.

I'm also very grateful for the support of my family and friends, who were there for me at all times.

Resumo

O cérebro humano é um sistema complexo capaz de gerar e integrar informação proveniente de diversas fontes. Estudos de conectividade cerebral têm vindo a abrir novos campos quer a nível experimental quer a nível teórico na área das neurociências. Certos métodos quantitativos integrados em estudos de redes neuronais podem ser prestáveis na caracterização de certas propriedades do cérebro, tais como: estrutural (dar forma à anatomia cerebral); fisiológico (estudar a resposta das interações; e sensorial, ao analisar a integração do cortex. Ao considerar o cérebro como uma rede complexa, os investigadores conseguem aceder a novos níveis de informação acerca do funcionamento cerebral a nível de memória, planeamento, raciocínio abstracto e patofisiologia.

Devido ao facto do sistema nervoso estar organizado em diversos níveis, é importante que este seja estudado e analisado usando mais do que uma técnica. As duas técnicas mais importantes que têm como principal objectivo aceder a informação de conectividade cerebral de modo não invasivo, são as seguintes: imagem de ressonância magnética por difusão; e imagem de ressonância magnética funcional. Qualquer um destes métodos possui as suas vantagens e desvantagens mas a principal diferença reside no facto de possuírem diferentes graus de sensibilidade a diferentes níveis de organização do cérebro.

Oscilações espontâneas do sinal dependente do nível de oxigénio sanguíneo (BOLD) em imagens de ressonância magnética obtidas com o sujeito em estado de repouso, já foram provadas ser importantes na identificação de redes funcionais no cérebro. Medidas de conectividade funcional obtidas com esta técnica são geralmente interpretadas como uma medida indirecta de actividade neuronal.

Este projecto consiste na investigação da relação entre espessura de determinadas regiões do cortex cerebral humano e a actividade neuronal espontânea derivada de sinais BOLD obtidos em estado de repouso. De modo a complementar este estudo,

para além das medidas de conectividade funcional, foram também obtidas medidas de conectividade estrutural, a partir de imagens de ressonância magnética de difusão, em particular o número de tractos neuronais ligados a cada uma das regiões de interesse, determinado a partir destas imagens. As outras medidas correlacionadas com a espessura cortical fazem parte das propriedades intrínsecas de redes “small-world” do cérebro e incluem o grau do nódulo, o coeficiente de aglomeração e o comprimento médio mínimo do trajecto, estimadas a partir da análise gráfica dos dados de ressonância magnética em estado de repouso.

As zonas activas do cérebro podem ser detectadas com ressonância magnética funcional que por sua vez mede oscilações no sinal BOLD. A contribuição do estado de repouso para este sinal está na ordem das baixas frequências ($0.01 - 0.1$ Hz). A conectividade funcional, definida como a correlação temporal (ou associação estatística) do sinal BOLD entre regiões distintas do cérebro foi obtida para um total de sessenta e oito regiões de interesse, para vinte e dois sujeitos. Os resultados destas correlações são apresentados em matrizes de conectividade funcional (68×68).

Devido ao facto de que correlações mais altas apresentam um nível de confiança maior, principalmente porque correlações fracas podem dar origem a falsos positivos, foi aplicado um limite mínimo arbitrariamente escolhido às matrizes de conectividade funcional, dando origem, desta forma, a um estudo paralelo, que dá maior importância às correlações mais fortes.

As medidas de espessura cortical tal como as máscaras das regiões de interesse foram obtidas a partir de imagens estruturais de ressonância magnética (T1), submetidas aos processos semi-automáticos do software FreeSurfer.

O desenvolvimento e crescimento de técnicas de ressonância magnética de difusão têm sido uma contribuição enorme ao nível da imagem neuronal, em particular por proporcionarem um método de estudo da conectividade estrutural do cérebro humano in vivo. A partir de imagens ponderadas em difusão é possível determinar a orientação das fibras que constituem a matéria branca do cérebro, ao detectar a difusão de moléculas de água que ocorre ao longo destas. Uma das técnicas associada à imagem por difusão é a tractografia, a partir da qual é possível determinar a continuidade de uma determinada fibra, voxel a voxel. Desta forma, é possível

quantificar conectividade estrutural (ou anatómica) ao acompanhar fibras que ligam determinadas regiões do cérebro. Neste projecto, o software DTK foi utilizado para determinar os tractos em todo o cérebro, a partir de imagens de difuso referentes a dezoito sujeitos. A partir deste ficheiro e das máscaras das regiões de interesse, foi possível calcular o número de feixes que ligam cada de região e desta forma construir matrizes de conectividade estrutural.

O campo matemático de “graph theory” proporciona a caracterização quantitativa de propriedades abstractas de sistemas complexos tal como o cérebro e permite também a obtenção de medidas que determinam a estrutura das redes neuronais. O primeiro passo para definir um gráfico consiste em estabelecer os nódulos, que são as regiões de interesse neste caso, e as ligações, construindo assim uma matriz de conectividade. Existem diversas medidas que podem ser obtidas a partir destas matrizes sendo que as mais importantes incluem: o grau do nódulo (número de ligações de um nódulo em particular); o comprimento do trajecto entre dois nódulos; e medidas que determinam o grau de agrupamento dos nódulos (“clustering”).

Tanto os coeficientes de correlação resultantes entre a espessura cortical e as medidas de conectividade funcional, conectividade estrutural e as propriedades de redes “small-world” do cérebro, como os resultados do teste t aplicado a estes, sugerem a não existência de qualquer tipo de relação entre estas variáveis. A única excepção foi o valor de correlação negativa ($r = -0.304$) entre a espessura cortical e o comprimento médio mínimo do trajecto, que apresenta significância estatística para um intervalo de confiança de 95%.

Para além destes resultados, existem ainda algumas observações que deveriam ficar retidas, tais como: as medidas de conectividade funcional mais fortes são observadas entre regiões simétricas a nível inter-hemisférico; o facto de limitar as matrizes que conectividade funcional não levar a resultados diferentes; as matrizes de conectividade funcional e as medidas de “graph theory” aplicadas a estas, sugerem a existência de propriedades de rede “small-world”, tal como seria esperado; e o facto de que as matrizes de conectividade funcional e estrutural serem tão, sugere a existência de ligações anatómicas directas e indirectas.

Palavras-Chave: conectividade; funcional; estrutural; cérebro; difusão; redes neuronais

Abstract

The human brain is an intricate system capable of producing and integrating information from various sources. Brain connectivity studies have been opening new experimental and theoretical fields in the area of neuroscience. Quantitative methods of network science can be helpful in characterizing certain brain properties, such as: architectural (shaping brain anatomy), physiological response by understanding network interactions and sensory features by analyzing cortex integration.

Spontaneous fluctuations of the blood oxygen level dependent (BOLD) signal in resting state functional magnetic resonance imaging have been proven to be important for the identification of functional networks within the brain. Functional connectivity measures obtained using this technique are generally interpreted as an indirect measure of neuronal activity.

The main goal of this project was to investigate how spontaneous neuronal activities in the human brain derived from resting-state BOLD signals relate with cortical thickness. In order to complement the study, the same relation was investigated for DTI data (number of tracks per region, in particular) and intrinsic properties of small-world networks (node degree, clustering coefficient and mean minimum path length) estimated using graph analysis on resting-state fMRI data.

The active parts of the brain are detected by fMRI with measures fluctuations in the BOLD signal. The resting-state contribution for this signal is known to be of low frequency ($\sim 0.01 - 0.1$ Hz). Functional connectivity, defined as the temporal correlation (or statistic association) of the signal between structurally distinct brain areas were assessed for a certain number of ROIs. A seed based method was used for this type of analysis. The cortical thickness measurements as well as the region of interest masks (total of 68) were obtained from the structural scans, using the

semi-automated procedures of the FreeSurfer software.

Because stronger correlations are more reliable, as weak links may stand for spurious connections, an absolute and arbitrary threshold was applied to the functional connectivity matrices, for a parallel study, regarding only stronger correlations.

The correlation coefficient calculated between cortical thickness and the measures of functional connectivity, structural connectivity and small-world properties of the brain and the t-test applied to them, suggests the non existence of a relation between them. The exception was the minimum path length that resulted in a correlation coefficient of $r = -0.304$ that presented significance for a 95% confidence interval.

Keywords: brain connectivity; functional; resting state; cortical thickness

Contents

| | |
|---|------------|
| Acknowledgements | i |
| Resumo | iii |
| Abstract | vii |
| Acronyms | x |
| 1 Introduction | 1 |
| 2 Theoretical Background | 5 |
| 2.1 The Brain | 5 |
| 2.1.1 Cerebral Cortex | 5 |
| 2.1.2 White Matter | 6 |
| 2.2 Brain Networks | 6 |
| 2.2.1 Brain Connectivity | 7 |
| 2.2.2 Graph Theory | 7 |
| 2.3 MRI Principles | 10 |
| 2.3.1 fMRI and BOLD Contrast | 10 |
| 2.3.2 Resting-State Functional Connectivity | 13 |
| 2.3.2.1 Analysis Methods | 15 |
| Seed Based Method | 16 |
| Independent Component Analysis | 17 |
| 2.3.3 Diffusion MRI | 18 |
| 2.3.3.1 Tractography | 20 |
| 3 Methods and Software | 23 |
| 3.1 Software | 23 |
| FreeSurfer | 23 |

| | |
|---|-----------|
| Statistical Parametric Mapping | 24 |
| Conn | 24 |
| Diffusion Toolkit and TrackVis | 25 |
| 3.2 Methods | 25 |
| 3.2.1 Cortical Thickness and ROI extraction | 25 |
| 3.2.2 fMRI preprocessing | 27 |
| 3.2.3 First-Level Analysis | 28 |
| 3.2.4 Statistical Analysis | 31 |
| 3.2.5 Graph Theory Analysis | 32 |
| 3.2.6 Structural Analysis | 33 |
| 4 Results and Discussion | 37 |
| 4.1 Cortical Thickness | 37 |
| 4.2 First-Level Analysis | 40 |
| 4.3 Statistical Analysis | 41 |
| 4.4 Graph Theory Analysis | 46 |
| 4.5 Structural Analysis | 52 |
| 5 Conclusion | 55 |
| References | 57 |
| Appendices | 65 |
| A Cortical thickness | 66 |
| B Correlation Coefficient Maps | 69 |
| C Statistical Analysis Plots | 73 |

List of Figures

| | | |
|-----|---|----|
| 2.1 | Scheme detailing the difference between ROIs and graph representations. The distance between nodes A and C is 4. The degree of node A is 2, B is 4 and C is 1. Node A is part of node B's neighbourhood, but C isn't, because they don't have a direct connection (Margulies et al., 2010). | 8 |
| 2.2 | Oxygenated and deoxygenated hemoglobin relative concentrations after a stimulus (Huettel et al., 2008) | 12 |
| 2.3 | fMRI task-activation study and resting-state study comparison (Biswal et al., 1995) | 14 |
| 2.4 | Functional connectivity measurement (van den Heuvel and Pol, 2010) | 14 |
| 2.5 | Isotropic and Anisotropic diffusions and eigenspace | 19 |
| 2.6 | Scheme for the streamline tractography approach. | 21 |
| 3.1 | Freesurfer surface and parcellation reconstructions | 26 |
| 3.2 | Registration | 28 |
| 3.3 | Preprocessing: rs-fMRI and T1 weighted structural image | 29 |
| 3.4 | Realignment parameters file | 29 |
| 3.5 | Preview results for one subject, including four ROIs. | 30 |
| 4.1 | Correlation coefficient map for subject one. | 40 |
| 4.2 | Left: Comparison of the time-series between the middle temporal ROI of the left (blue) and right (red) hemispheres, for subject one; Right: Comparison of the time-series between the lateral occipital (blue) and parahippocampal (red) ROIs, of the right hemisphere, for subject one | 41 |

| | | |
|------|--|----|
| 4.3 | Left: relation between the cortical thickness and the maximum correlation coefficient for every subject and Right: relation between cortical thickness and the five highest values of the correlation coefficients for every subject. | 42 |
| 4.4 | Relation between the cortical thickness correlation coefficient for the: (Upper Left) Rostral Middle Frontal; (Upper Right) Rostral Anterior Cingulate; and (Bottom) Precentral. | 43 |
| 4.5 | Average correlation coefficients and cortical thickness by subject for: (Left) all data; (Right) only positive correlations. | 44 |
| 4.6 | Average correlation coefficients and cortical thickness by ROI for: (Left) all data; (Right) only positive correlations. | 45 |
| 4.7 | Correlation matrices visualized in anatomical space, for: (Left) No threshold; (Middle) Threshold at 0.2 and; (Right) Threshold at 0.4. The top images are presented in posterior coronal view, and the bottom ones in superior axial. | 50 |
| 4.8 | Degree K of each ROI against their cortical thickness, for the three different thresholds. | 50 |
| 4.9 | Clustering coefficient C of each ROI against their cortical thickness, for the three different thresholds. | 51 |
| 4.10 | Mean minimum path length L of each ROI against their cortical thickness, for the three different thresholds. | 51 |
| 4.11 | Visualization of the tracks file for subject one: (Left) sagittal; (Middle) anterior coronal and (Right) superior axial. | 52 |
| 4.12 | Structural connectivity matrix for subject one. | 52 |
| 4.13 | Average structural connectivity and cortical thickness per: (Left) subject; (Right) ROI. | 53 |
| B.1 | Correlation coefficient map for subjects one to four. | 69 |
| B.2 | Correlation coefficient map for subjects five to ten. | 70 |
| B.3 | Correlation coefficient map for subjects eleven to sixteen. | 71 |
| B.4 | Correlation coefficient map for subjects seventeen to twenty-two. . . . | 72 |

| | | |
|-----|---|----|
| C.1 | Average correlation coefficients and cortical thickness by subject (using the whole data), applying a threshold of: (Top Left) 0.2; (Top Right) 0.4; (Bottom Left) 0.6; and (Bottom Right) 0.8. | 73 |
| C.2 | Average correlation coefficients and cortical thickness by subject (using only the positive correlations), applying a threshold of: (Top Left) 0.2; (Top Right) 0.4; (Bottom Left) 0.6; and (Bottom Right) 0.8. . . . | 74 |
| C.3 | Average correlation coefficients and cortical thickness by ROI (using the whole data), applying a threshold of: (Top Left) 0.2; (Top Right) 0.4; (Bottom Left) 0.6; and (Bottom Right) 0.8. | 75 |
| C.4 | Average correlation coefficients and cortical thickness by ROI (using only the positive correlations), applying a threshold of: (Top Left) 0.2; (Top Right) 0.4; (Bottom Left) 0.6; and (Bottom Right) 0.8. . . . | 76 |

List of Tables

| | | |
|-----|---|----|
| 4.1 | Cortical thickness (mm) of 68 ROIs (left and right hemispheres) for three subjects | 38 |
| 4.2 | Correlation values between cortical thickness and functional connectivity for all study cases. | 46 |
| 4.3 | Cortical thickness (mm), degree (K), clustering coefficient (C) and characteristic path length (L), for each region of the left hemisphere, estimated from three correlation matrices, differing only in the threshold used. | 47 |
| 4.4 | Cortical thickness (mm), degree (K), clustering coefficient (C) and characteristic path length (L), for each region of the right hemisphere, estimated from three correlation matrices, differing only in the threshold used. | 48 |
| 4.5 | Scalar results that estimate the small-worldliness of a network. . . . | 49 |
| A.1 | Cortical thickness (mm) of 68 ROIs (left and right hemispheres) for subjects one to eleven. | 67 |
| A.2 | Cortical thickness (mm) of 68 ROIs (left and right hemispheres) for subjects twelve to twenty-two | 68 |

Chapter 1

Introduction

The brain is basically constituted by gray matter structures connected to other gray matter areas or other brain structures by white matter tracts. This way we can think of the brain as a network composed by several areas that perform different tasks and functions, but are continuously sharing information with each other. This interchange of information describes the brain function.

In the past decades, neuroimaging studies have provided essential knowledge about the structure and function of the brain regions of the primate and human brains and the more recent advances in functional neuroimaging allowed researchers to measure and examine functional interactions between brain areas that lead to the studies of functional connectivity in the human brain. Roughly speaking, the information gathered from studies focusing on the activity of discrete brain regions were complemented with results from studies looking at the interaction between these different brain areas.

Most of the information available about the anatomic connectivity of the human brain was obtained from studies that either used invasive techniques in non-human primates or made inferences from human brain lesions (Dijk et al., 2010). Some studies also used postmortem tracing techniques, but they are limited to short distance connections. These are the main reasons why noninvasive human techniques based on MRI have been growing in interest and have shown a significant development.

Noninvasive mapping of the human brain connectivity is normally assessed by two main MRI techniques: diffusion tensor imaging (DTI) and functional connectivity MRI (fcMRI). The basic principle of DTI is that by measuring water diffusion in

multiple directions, it is possible to estimate the location and trajectories of axonal bundles and therefore reconstruct the pathways using MRI. On the other hand, functional connectivity can be defined as the “temporal dependency of neuronal activation patterns of anatomically separated brain regions” (van den Heuvel and Pol, 2010), in other words it is based on the correlation of time series data from independent brain regions, and it is believed to reflect functional communication between brain regions (Biswal et al., 1995)(Cordes et al., 2000). Because these measurements are often obtained while the subject is at rest, the method is often referred to as resting-state functional connectivity (RSFC) and the identified brain networks as resting-state networks (RSN).

The analysis of resting-state data has the advantage of focusing the study on endogenous or background neurophysiological processes, however, the principal disadvantage is the incomplete understanding of the generative mechanisms and cognitive significance of endogenous, correlated oscillations in fMRI data (Achard et al., 2006).

Functional connectivity methods are currently being applied to various areas such as cognitive psychology, clinical diagnosis and treatment progression, but although some of them yielded promising preliminary results, the researchers still have to surpass all the methodological and interpretative issues inherent to this rapidly advancing field.

The development and evolution of MRI techniques regarding DTI are a important contribution to the neuroimaging field, in particular, by providing a method to study structural connectivity in vivo in humans. Diffusion weighted imaging (DWI) can characterize the orientation of white matter (WM) fiber bundles by detecting underlying water molecules diffusion (Gong et al., 2009). In particular, tractography methods (or fiber tracking methods) that use the deterministic streamline technique can infer the continuity of fiber bundles from voxel to voxel (Mori et al., 1999; Gong et al., 2009). This way, it is possible to quantify structural (or anatomic) connectivity by tracking WM bundle pathways that link to cortical regions (Guye et al., 2008).

Lately, there have been developments in the study of brain network organization, by means of graph theory. The basic representation of a graph is obtained from the

connectivity matrices (either functional or structural). I defines the topology of the graph by setting the nodes as matrix rows and the links as binary or weighted matrix entries. There are various measures that can be obtained from these graph, but the most important and widely used for brain network studies include the node degree, the path between nodes and measures of segregation.

The main goal of this project is to study the relation between cortical thickness and functional connectivity from resting-state fcMRI. From the outcomes of this study it will be possible to analyze if the functional connectivity is somehow affected by the thickness of the cortex. Although cortical thickness and resting-state functional connectivity are both well documented, until now there haven't been any efforts to relate the two of them.

Usually, when studying the brain, only one technique is not sufficient to fully understand how it is organized. For this reason two additional and complementary studies were performed as well. These comprised structural connectivity by means of DTI and tractography and a group of brain networks measures, such as node degree, clustering coefficient and mean minimum path length. Again, the relation between cortical thickness and the results of these measures was the goal of the study.

The structure of this thesis comprises several chapters. Chapter 2 presents the theoretical background of this project, including an introduction to the brain (section 2.1) and to brain networks (section 2.2) with graph theory and an overview of the MRI principles (section 2.3) comprising functional MRI, resting-state functional connectivity, diffusion MRI and tractography. In chapter 3 the software relevant to this project is going to be presented, together with the methods and techniques used to process and analyze the data. In chapter 4 the results are presented and discussed and the conclusion is provided in chapter 5.

Chapter 2

Theoretical Background

This chapter presents an overview of all the topics relevant to the understanding of this project. It includes: an introduction to the brain (section 2.1); and to brain networks (section 2.2) including an approach to graph theory; and a synopsis of the MRI principles (section 2.3) comprising functional MRI, resting-state functional connectivity, diffusion MRI and tractography.

2.1 The Brain

2.1.1 Cerebral Cortex

The importance given to the cerebral cortex is laid on the fact that it performs the brain operations responsible for the cognitive abilities (Kandel et al., 2000).

The cortex is divided in two hemispheres and consists in the outermost layer of the brain. Each hemisphere is responsible for the sensory and motor processes of the contralateral side of the body. It is important to note that the hemispheres are not symmetric either in structure nor function. The characteristic grey colour of the cortical layer, grey matter, is the result of it being composed by unmyelinated neuronal cell-bodies; on the other hand, the white matter that is present throughout the rest of the brain consists of myelinated axons. The fact that the cortical layer also contains blood vessels is important for functional MR imaging, but this will be explained in the next section. The thickness of the human cortex varies between 1.5 and 4.5 mm (Kandel et al., 2000) and can be measured from structural MRI (Fischl and Dale, 2000).

The cortex contains many foldings, the parts that go into the brain are called

sulci and the visible parts of the folds are called gyri. The surface area of the brain is about 2300 cm^2 (Kandel et al., 2000), but most of it is confined within the sulci, caused by an evolutionary strategy for spatial efficiency.

The cerebral cortex can be divided both anatomically and functionally. The anatomic division consist in the frontal, temporal, parietal and occipital lobes. Each of these regions is known to have specialized functions.

The functional division is far more complex, mainly because there can be more than one region of the brain that takes part in the same functional activity. Some examples of the most documented functional regions are the primary motor cortex (frontal lobe), somatosensory cortex (parietal lobe), primary visual cortex (occipital lobe) and the auditory processing areas (temporal lobe).

2.1.2 White Matter

As it was said in the previous section, The white matter of the brain is mostly constituted by myelinated axons. It is believed that these axons are responsible for the transmission of information between cortical areas and between the brain and other parts of the human body.

Brain hodology is the discipline responsible for the study of the anatomy of fibers that connects remote cerebral regions. Information has been gathered along the years as the result of invasive tracing studies of the non-human primate and postmortem and in vivo virtual dissections of the human brain (Jones, 2010).

There are various types of white matter fibers, but roughly they can be classified into three groups: projection, commissural and association fibers. Projection fibers compose the ascending and descending pathways that have origin or terminate in the cortex, commissural fibers connect the cortex between the two cerebral hemispheres and association fibers connect cortical regions within a hemisphere.

2.2 Brain Networks

An expanded knowledge about network interactions at various levels of organization is crucial for an understanding of the brain as an integrated system (Sporns, 2011).

2.2.1 Brain Connectivity

Brain connectivity studies have been opening new experimental and theoretical fields in the area of neuroscience, mostly because of its importance in neuroanatomy. Quantitative methods of network science can be helpful in characterizing certain brain properties, such as: architectural (shaping brain anatomy), physiological response by understanding network interactions and sensory features by analyzing cortex integration. Other properties of the brain can also be studied by analyzing the variation between healthy subjects and patients, across healthy subjects and over time (ageing).

There are many different ways of describing and measuring brain connectivity, each one depending on the method used to observe the brain and the way how the neural data is processed. The two most important methods are structural and functional connectivity which despite their differences are believed to be interdependent. Structural connectivity refers to the physical or anatomical connections linking neural elements while functional connectivity refers to the statistical independence between distributed and often remote brain regions (Sporns, 2011). Both of these methods are going to be explained in more detail in further sections of this chapter. Another important method is effective connectivity which is not going to be explained in detail since it is not within the scope of this project.

In order to fully understand how brain networks operate one needs to apply more than one mode of brain connectivity. Structural and functional brain networks can be constructed from empirical data by following a certain number of steps. First of all the network nodes need to be defined as well as the measure of association between pairs of nodes. These association estimates are then arranged in an association matrix, which can be thresholded or not depending if the scope of the study is strong associations. Finally, it is possible to apply statistical or graph measures to these matrices in order to infer on the properties of the brain network.

2.2.2 Graph Theory

The mathematical field of graph theory allows the quantitative characterization and mapping of abstract properties of complex systems, such as brain systems. In

this project the graph analysis is based on measures of brain networks.

Graph theory can be applied to the brain by designating the ROIs (or single voxels) as the nodes, and the connections between them as the edges. In this way it is possible to use the knowledge of graph theory to analyse functional brain networks (see figure 2.1). The most basic representation of a graph is the adjacency matrix, or connection matrix. It defines the topology of the graph by representing nodes as matrix rows and columns and the links as binary or weighted matrix entries; examples of adjacency matrices are given in figure 4.1 and appendix B.

One of the most fundamental graph measures is the degree. The degree of a node is the number of links connected to it. The degree distribution (degree of all nodes) shows whether node degrees are approximately the same or if it varies over a broader range and offers information about the number of nodes which have a very high degree, termed “hubs”. The neighbourhood of a node is the sum of nodes that connect to it directly by one edge.

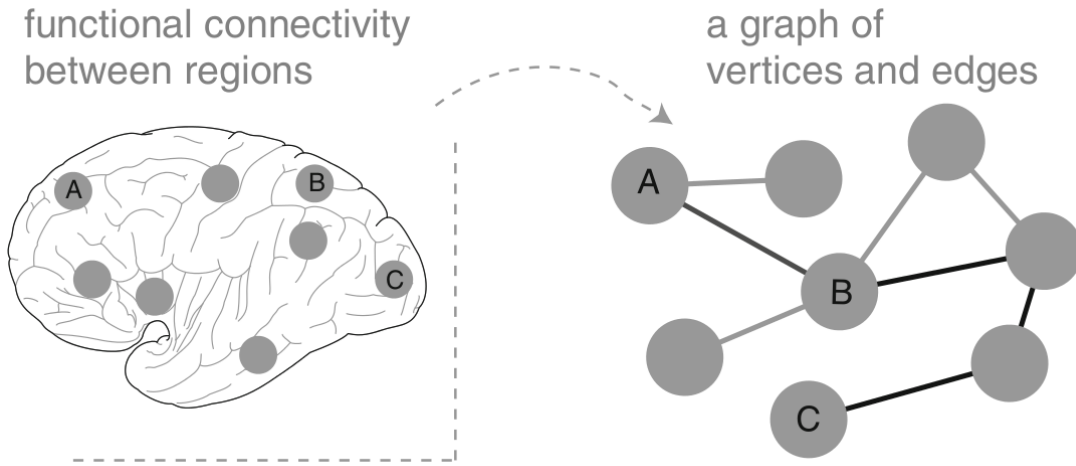


Figure 2.1: Scheme detailing the difference between ROIs and graph representations. The distance between nodes A and C is 4. The degree of node A is 2, B is 4 and C is 1. Node A is part of node B’s neighbourhood, but C isn’t, because they don’t have a direct connection (Margulies et al., 2010).

A path is defined as a sequence of succeeding nodes connected by edges, and the length of a path is the number of edges that compose it. In weighted graphs, the paths composed by stronger links span shorter distances. The distance between two particular nodes is the number of edges that traverse the shortest path possible. The average path length is the mean of all the distances between two particular

nodes and can be taken as a measure of how well integrated a graph is. Functional integration in the brain is the capability to swiftly combine specialized information from distributed brain regions. These measures are based in the estimation of the easiness of communication between brain regions by analysing the path between them.

Connection density is the fraction between the number of existing links in the graph and the total number of possible links.

Because the brain supports both modular and distributed processing of information, it makes sense to consider it as a small-world network (Bassett and Bullmore, 2006). A network with a small topology is most efficiently configured: high clustering supports modular processing and short distances support distributed processing, maximizing parallel processing, minimizing wiring costs and making it fault tolerant. All of these are optimal properties of a central nervous system (Margulies et al., 2010). Modularity describes how the brain network can be divided into separate components (modules) with high internal connectivity, but sparse inter-module connections. This type of measurement can be used to characterize a network as a small-world network.

Functional segregation in the brain is the capability of densely interconnected nodes to perform specialized processing. As a first step it is necessary to identify these groups, known as clusters or modules, within the network. The most simple measures of segregation are based on the number of triangles in the network, the higher the number of triangles the more implicit is the segregation. The fraction of triangles around a specific node is known as the clustering coefficient, in other words, it quantifies the number of connections that exist between the nearest neighbours of a node as a proportion of the maximum number of possible connections (Bullmore and Sporns, 2009). The local clustering coefficient can be used to measure the local structure of a graph and although some studies show that regular networks have a high clustering coefficient and a high path length, the small-world phenomenon implies both high clustering and short path distances (Stam and Reijneveld, 2007).

The vulnerability of a graph can be explored with random error and target attack by using the degree distribution. The random error technique repeatedly deletes a

random node, while the target attack does the same thing but always to the node with the highest degree. After each iteration, the vulnerability of the graph can be determined by using a variety of tools: clustering coefficient, average path length, small-world properties, and local and global efficiency (Margulies et al., 2010). This technique is of particular importance because it permits us to know if, a lesion occurs in a certain area of the brain, the connection between regions will be disrupted or not.

2.3 MRI Principles

2.3.1 fMRI and BOLD Contrast

Functional magnetic resonance imaging (fMRI) is a neuroimaging technique that explores changes in brain function/metabolism over time, using the standard MRI scanner (use of strong magnetic fields to create images of biological tissues). Its' development gave origin to a new wave of functional neuroimaging studies.

When one thinks about the functional neuroimaging methods, it is important to remark that these don't directly measure neuronal activity but do actually measure the metabolic necessity of the active neurons. Since the brain has poor energy stocks it is continuously supplied by the blood. It is the change of blood flow responding to the need of oxygen and glucose by neurons that results in a signal that can be measured by fMRI.

One of the important factors related to this type of contrast is whether the blood is oxygenated or not. The hemoglobin molecule has magnetic properties and it can be either diamagnetic or paramagnetic depending if it is oxygenated (oxyhemoglobin or Hb) or deoxygenated (deoxyhemoglobin or dHb), respectively. The difference between these two states is that if it's diamagnetic it has no magnetic moment and if it is paramagnetic it has a magnetic moment and can be attracted to a magnetic field. When the hemoglobin molecules lose their oxygen to neurons there is an increase of the magnetic susceptibility that will cause the spins to dephase in the presence of the magnetic field of the MRI scan. This dephasing will result in a decay of the transverse magnetization and thus will be detected by MR pulse sequences sensitive

to T_2^* . This technique is called in fMRI as the blood-oxygenation-level dependent (BOLD) contrast.

The reason why BOLD is so important is because it is believed to measure changes due to brain activity. There are two main reason for these changes: oxygen metabolism and blood flow. Neuronal activity demands oxygen causing an increase of deoxygenated hemoglobin while an increase in blood flow causes a decrease in deoxygenated hemoglobin.

Although the deoxygenated hemoglobin decreases the MR signal, there is a stronger signal in active parts of the brain. To explain this fact, scientists think that there is more supplied oxygen to the brain than what is consumed. If a certain brain region becomes active there will be an increase of the deoxygenated hemoglobin concentration followed by a higher (about three times) increase of oxygenated hemoglobin as shown on figure 2.2.

Albeit all the controversy about the true origin of the fMRI signal, it is a fact that changes in blood oxygenation can be measured using MRI. This resulting signal is known as the hemodynamic response (HDR). The hemodynamic response is the change in MR signal on T_2^* images following local neuronal activation and is caused by a decrease in the amount of deoxygenated hemoglobin present within a voxel.

Neuronal activity results in an increase in the BOLD signal, but researchers have observed a small decrease in the MRI signal (due to an increase in deoxygenated hemoglobin) before the positive change. This decrease in MR signal is normally found in voxels that have a good spatial correspondence with active neurons. On the other hand the positive change results in a more spatially diffuse and extended signal. One explanation for these differences is that the neuronal activation causes a decrease oxygenation in nearby capillaries followed by an overcompensatory oxygenated blood delivery in the surrounding area. Although the initial decrease in MR signal appears to be of high importance, it is rarely mentioned in the majority of fMRI studies.

Regarding functional MR images it is important to have an idea of the parameters that make it possible to assess the data and infer results. One of these parameters is spatial resolution, and in fMRI it depends on the voxel size which is determined by the field of view, matrix size and slice thickness. In functional imaging voxel size

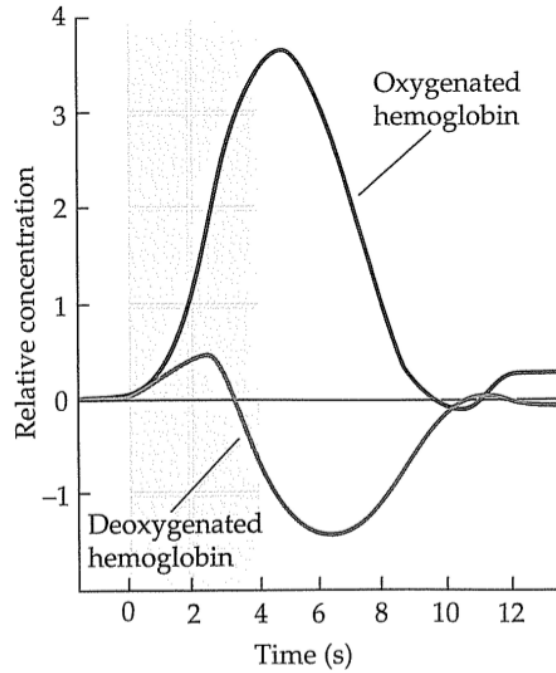


Figure 2.2: Oxygenated and deoxygenated hemoglobin relative concentrations after a stimulus (Huettel et al., 2008)

tends to be larger, for the whole brain compared to standard anatomical images. The two main reasons why larger voxels are used in this kind of image are the increased signal-to-noise ratio and the decreased acquisition time which is essential to enable the acquisition of a large number of time points (each sampling the whole brain) within practical acquisition times.

In most of the fMRI studies, including the one in question, temporal resolution has a high importance. It is important to know when did things exactly happen and so functional MRI has a temporal resolution that can identify different events separated temporally by a few seconds. Temporal resolution is defined by the repetition time (TR), the same way that the voxel size defines spatial resolution. Because the hemodynamic response is continuous and takes longer than the neuronal activity itself, normally TRs of about one to two seconds are enough to fully estimate this response.

One last thing that is important to note, is that most times, the activity changes of interest are mixed with other measurements. There are various sources of variability that can mask the BOLD effect. The most important include: temperature, physiological effects (heart and respiratory rates) and head motion. The effects of

this unwanted variability can be minimized by a series of preprocessing steps to the fMRI data (which are going to be explained in detail in section 3.2.2).

2.3.2 Resting-State Functional Connectivity

The main purpose of the resting-state functional connectivity (RSFC) approaches is to delineate, study and explore distinct functional networks in the brain by measuring the level of co-activation of resting-state fMRI time-series between brain regions. Related research has revealed impressive new findings about the functional connectivity between brain areas and local networks. One of the most stimulating outcomes is the new perspective of the overall organization of functional communication in the brain network (van den Heuvel and Pol, 2010).

Functional connectivity data can be assessed through a number of steps, as was first described by Biswal et al, in his study concerning the activation of the motor cortex during rest. The first step in his study was to acquire fMRI data while the subject was “at rest” in the scanner, performing no explicit task. Afterwards the subject was asked to move the fingers of both hands and the data obtained was analyzed for activation. In this procedure, activity should be detected in both the left motor cortex and right motor cortex, as seen in figure 2.3a. The next step is to extract the timecourse of the left motor cortex from the data that was collected at rest. When this time course is correlated with the rest of the brain by the means explicit in figure 2.4, similar timecourses are detected in very specific parts of the brain 2.3b. From this data, researchers can obtain information about the structure and basic organization of the brain.

Usually, if the study is to assess a particular mental process, the researchers complement the resting-state data with anatomical or diffusion MR images associated with a certain task. This kind of study has been applied for studying several mental functions such as motor activity, language perception, visual perception, reading and memory.

Resting-state networks consists of spatially distant, but functionally linked brain regions that show a high level of co-activation during rest. The way the measures are achieved is explained in figure 2.4. The time-series of the ROI is extracted and

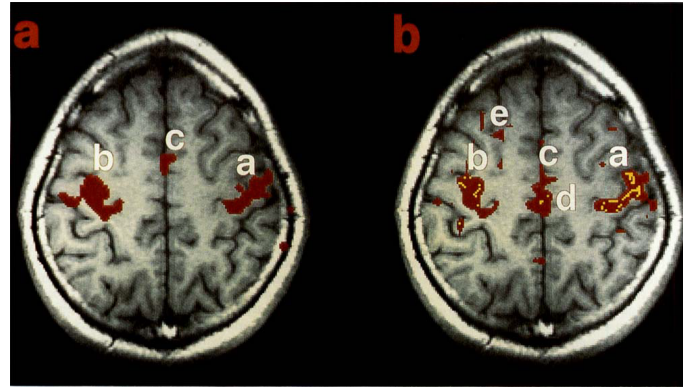


Figure 2.3: a) fMRI data from bilateral finger movement task-activation study. b) Resting-State functional connectivity data. In both studies the regions activated are fairly similar (Biswal et al., 1995).

then correlated with the time-series of the remaining voxels of the brain. The higher the correlation the more are the regions functionally connected. The functional connectivity map shows all the regions that have a certain level of connectivity with the selected seed.

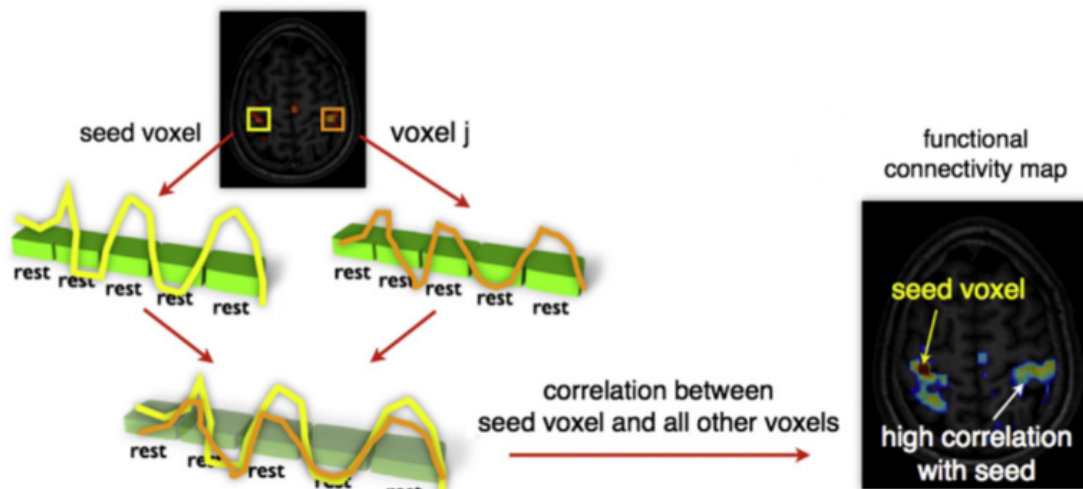


Figure 2.4: Functional connectivity measurement (van den Heuvel and Pol, 2010)

When comparing resting-state fMRI time-series between brain regions, there's the possibility that they might be anticorrelated. This means that periods of high activity of one region coincide with periods of low activity of another particular region.

Until now eight sub-networks have been found, which are commonly reported in studies, including language, visual and motor areas, that showed a high level of

functional connectivity between anatomically separated brain regions during rest (van den Heuvel and Pol, 2010).

It has been shown that the correlations and observed between brain regions in resting-state functional connectivity studies are driven by the spontaneous low frequency fluctuations ($\sim 0.01 - 0.1$ Hz) in the BOLD signal. In order to obtain this signal, a low-pass or more commonly, a band-pass filter is applied to the fMRI data, which automatically removes the respiratory ($0.1 - 0.5$ Hz) and cardiovascular ($0.6 - 1.2$ Hz) signal frequency contributions.

Various researchers have suggested that these signals fluctuations have their origins in functional resting-state networks (RSNs), localised to grey matter regions and that they characterize the neuronal baseline activity of the human brain in the absence of deliberate and/or externally stimulated neuronal activity, and may themselves reflect functionally distinct networks (Beckmann et al., 2005). Another theory is that resting-state networks may aid to keep functional systems in an active state, performing maintenance tasks that help improve performance and their reaction time whenever functional connectivity is needed. Indeed, recent studies have suggested that long term training may significantly increase resting-state activity within brain regions related to that activity (van den Heuvel and Pol, 2010). In the same line of thought, there have been reports that regions with a higher level of structural connectivity show a higher level of functional connectivity (Hagmann et al., 2008).

One of the advantages of resting-state studies over task-fMRI is that because it requires a low performance profile by the subject, it is possible to apply it to diseased or uncooperative populations (infants, sedated subjects or subjects with cognitive or physical impairments), although it might be harder to correct the effects of movement.

2.3.2.1 Analysis Methods

There are various methods for detecting functional connectivity from fMRI, but basically they can be inserted in one of two groups: model-dependent and model-free methods. The model-dependent is based on a seed region approach and the model-

free includes: principal component analysis (PCA), singular value decomposition (SVD), independent component analysis (ICA) and clustering (Cole et al., 2010; Lee et al., 2012; Huettel et al., 2008). Only the seed based method and the independent component analysis are going to be explained in more detail in this report and only the seed based method is actually going to be applied in the project.

Seed Based Method

The seed based method is a model-dependent approach. Normally the simplest way of applying this method is to define the ROI (seed) from the anatomical data, register it to the functional images, calculate the mean resting-state time-series for this region and correlate it with the time series for the rest of the brain voxels or a designated group of ROIs. Inside the seed based method this is known as the cross-correlation analysis (CCA). There are various ways to define a seed region: anatomically, from a predefined atlas, or from functional data. The anatomically defined seed region is drawn on the subject data according to their individual brain structure or to a standardized reference brain (the latter approach depends on the quality of the registration). The atlas-based approaches apply predefined atlases that have predefined anatomic structures already in a reference space. The seed region can also be defined from functional data based on task activations.

The main advantage of the seed based method over other methods is that it provides a direct answer to a direct question by providing a network of regions most strongly functionally connected with the seed ROI (Cole et al., 2010).

Regardless of the approach used for the seed selection, it will result in a functional connectivity map (fcMap) that provides us with the functional connections of the preselected brain region. The fcMap provides information both about which regions are functionally connected and the extent of these connections. The seed based method results in a fcMap that provides us limited information because it only correlates the time-series regarding the selected brain region. In order to identify the voxels that are significantly correlated with the seed, a threshold is applied to the functional images (Lee et al., 2012).

The ROIs used for this kind of seed based method are believed to reduce spatial

resolution by changing the unit from a single voxel to a region containing many voxels (Cole et al., 2010). But, if the ROIs are chosen carefully and correctly registered to the functional images, functional resolution will be increased by averaging many similar neighbor voxels (Cole et al., 2010). In fMRI studies it is common practice to take many analysis steps that sacrifice spatial resolution in order to increase functional resolution (Huettel et al., 2008).

If the main purpose is to study connection patterns at the scale of the whole-brain, model-free methods can be used. These methods allow the investigation of functional connectivity without a priori assumptions regarding regions of interest. One of these methods is the ICA which is described below.

Independent Component Analysis

The Independent Component Analysis (ICA) is the most commonly used of the model-free methods. Because it doesn't need any a priori information either from spatial nor temporal signal sources, it is ideal to use in resting-state fMRI studies. Researchers can choose between spatially or temporally independent components, depending on the study. When applied to the data, it searches for signal sources that are maximally statistically independent from each other. The resulting analysis may be more difficult to interpret than the fcMaps but it is the most efficient method for group comparison. It is also believed that the result obtained using ICA are less likely to have artefactual effects from noise.

The two main disadvantages of the ICA method are iterative optimisation used for its' decomposition (which induces a degree of run-to-run variability) and arbitrariness of the processes of dimensionality reduction and model order selection (the researcher has to define how many components are to be estimated).

Albeit both these methods have their inherent differences, disadvantages and advantages, they all tend to give fairly similar results (van den Heuvel and Pol, 2010).

2.3.3 Diffusion MRI

Diffusion MRI is a neuroimaging method capable of mapping the diffusion of water molecules across biological tissues. Diffusion itself can be defined as the free motion of molecules in a medium. This phenomenon is explained by Fick's first law:

$$J = -D\nabla C \quad (2.1)$$

where J is the net particle flux, C is the concentration and D is a constant of proportionality, called the diffusion coefficient. This law takes into account that the flow takes place from highly concentrated regions to regions with low concentration. The diffusion flux is proportional to the diffusion coefficient and to the concentration gradient and unlike the latter, the diffusion coefficient varies with the medium: its' value is determined by the size of the diffusing molecules, the temperature and the microstructural properties of the medium (which allow us to explore biological tissues). Even if on average there is no net flux, the particles are still moving and the distance they cover increases over time, according to Einstein's equation:

$$\langle r^2 \rangle = 6Dt \quad (2.2)$$

where r^2 represents the mean distance travelled by the particle after the elapsed time t and D is the diffusion coefficient for that particular particle. The probability of a particle to displace a given distance from the origin is the same, no matter which direction. The units of the diffusion coefficient are $mm^2 s^{-1}$ and for pure water at 37°C it's value is $2.2 \times 10^{-3} mm^2 s^{-1}$ (McRobbie, 2007).

Magnetic resonance, specifically the spin-echo MR signal, is sensitive to molecular diffusion, which provides the possibility to quantify the diffusion characteristics of various molecules. By the application of gradients, the spins in different locations will gain different phase shifts. In diffusion MRI the b -value characterizes the sensitivity to diffusion and it is proportional to the gradient strength.

Nowadays the most commonly used sequence is the pulse gradient spin-echo introduced by Stejskal and Tanner (PGSE). To be able to calculate the diffusion coefficient properly at least two signals from the same sample are needed, the

diffusion-attenuated signal, $S(b)$, and the signal in the absence of any gradients $S(0)$. It is important to remark that in the presence of diffusion, there is a loss of signal. These two quantities relate to the diffusion coefficient D in the following way:

$$\ln \left[\frac{S(b)}{S(0)} \right] = -b \cdot D \quad (2.3)$$

This equation is applied to all the voxels of the volume and afterwards it is possible to obtain an apparent diffusion coefficient (ADC) map. In this type of images, the brighter the voxel the higher is the diffusion coefficient.

The pulse gradient spin-echo is only sensitive to diffusion that occurs in the same direction as the applied gradient. Within one scan various images corresponding to diffusion gradients applied along different directions (for example: x , y and z) can be acquired and for each one of them an ADC is computed. If the mean of these ADCs is calculated for each voxel, it is possible to obtain the mean diffusivity.

The application of multiple gradient is the basic requirement for diffusion tensor imaging (DTI). If the ADC is the same along all directions within a particular region, the diffusion is isotropic, but if the diffusion has a preferential direction it is said to be anisotropic, this difference is shown on figure 2.5, on the left. The brain regions that reflect a high degree of anisotropy are within the white matter and the main cause for this anisotropy is believed to be the presence of myelin (Ciccarelli et al., 2008; Bihan et al., 2001; Gong et al., 2009; Guye et al., 2008).

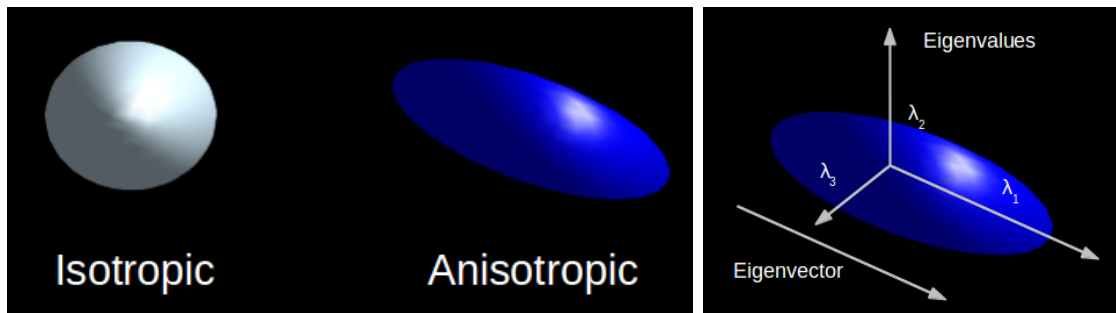


Figure 2.5: Left: Difference between isotropic and anisotropic diffusion; Right: Eigenvalues and Eigenvector.

The diffusivity can be characterized by the eigensystem (reference frame), composed by three axes, each one of them represented by an eigenvector, and their lengths

are given by the diffusion distance in a given time - figure 2.5 on the right. The orientation of the diffusion tensor is parallel to the principle eigenvector, which is the biggest, meaning it represents the preferential diffusion direction. This orientation is assumed to be the same as the fiber in question.

From the eigenvalues it is possible to calculate two other measures that quantify the directional variability of the diffusivity, the fractional anisotropy (FA) and the relative anisotropy (RA), given by:

$$FA = \sqrt{\frac{3}{2} \frac{\sqrt{(\lambda_1 - \langle \lambda \rangle)^2 + (\lambda_2 - \langle \lambda \rangle)^2 + (\lambda_3 - \langle \lambda \rangle)^2}}{\sqrt{\lambda_1^2 + \lambda_2^2 + \lambda_3^2}}} \quad (2.4)$$

and

$$RA = \sqrt{\frac{1}{3} \frac{\sqrt{(\lambda_1 - \langle \lambda \rangle)^2 + (\lambda_2 - \langle \lambda \rangle)^2 + (\lambda_3 - \langle \lambda \rangle)^2}}{\langle \lambda \rangle}} \quad (2.5)$$

The FA measures the portion of the tensor that relates to anisotropic diffusion and because it is normalized, the values are between zero (isotropic diffusion) and one (anisotropic diffusion). It is possible to show these results on a map, where the FA values near to one are the brightest.

Summing up, the key parameters in diffusion tensor imaging (DTI) are the mean diffusivity, the fractional anisotropy and the direction of maximum diffusion.

2.3.3.1 Tractography

Another key feature of diffusion MR is the possibility to perform tractography, which is a method (non-invasive and in-vivo) that allows the identification of white matter pathways within a brain. These pathways are believed to be highways of information transfer between brain regions.

The most important assumption of diffusion tractography is that the water molecules will diffuse to a greater extent along the axons (longitudinally). There are various algorithms for tractography and each of them provides a different interpretation for the reconstruction of the pathways and their connectivity indices.

The streamline is the most commonly used algorithm. From a seed voxel, a pathway is built by connecting voxels accordingly to their maximum diffusion direction, as can be seen in figure 2.6. There can be applied some constraints such as an angular threshold or an anisotropy threshold. The angular threshold is applied because sharp direction changes are highly unlikely to occur in brain connections and the anisotropy threshold is applied because low values don't correspond to white matter. Streamlines are then computed by seeding every voxel in the brain, but only the ones that meet certain anatomical criteria, are retained.

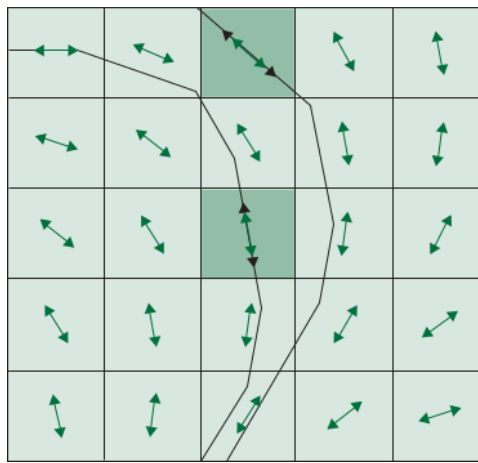


Figure 2.6: Scheme for the streamline tractography approach (Ciccarelli et al., 2008).

Fiber bundles (major white matter tracts) can be properly isolated and delineated by defining two ROIs. The streamlines that pass through both these ROIs are said to be part of the same fiber. White matter tracts for which a larger number of streamlines could be found are believed to relate to a stronger structural connectivity.

Chapter 3

Methods and Software

In this chapter a list will be given of the software relevant for this project, including a brief explanation of the methods each one of them uses. The next sections will detail a list of the steps taken to analyze the data within this project.

3.1 Software

Two software packages (FreeSurfer and SPM) and a toolbox (Conn) were used to process the anatomical (T1-weighted) MR images and functional data. The Diffusion toolkit and TrackVis, on the other hand, were used to process the DTI data. Each software performs a different task within the project.

FreeSurfer

FreeSurfer (surfer.nmr.mgh.harvard.edu) is an open source software package used to, among other things: create brain models from MRI; process fMRI data; measure certain properties of the brain, including cortical thickness and regional volumes.

The cortical thickness is measured automatically, for the whole brain, using a built in method. It is calculated by determining the distance between the gray/white and pial surfaces created by the surface reconstruction (Fischl and Dale, 2000).

The cortical surface reconstruction given by FreeSurfer is obtained from automated procedures. It runs the T1 weighted images through a series of steps. First it registers the images to a template volume provided by FreeSurfer itself, and saves the coordinates. Then, in order to minimize the effect of magnetic susceptibility artefacts and radio-frequency field inhomogeneities, an intensity normalization is

applied to the images. The next step applies an automated process for stripping the skull from the images.

Because the resolution of MRI is not always sufficiently high, the pial surface is difficult to define directly. Instead, the gray/white boundary is computed and deformed outwards to find the pial surface (Dale et al., 1999). Roughly speaking, the segmentation process distinguishes tissues based on their intensity information.

One of the key features of FreeSurfer is that it automatically parcellates the human cerebral cortex, assigning neuroanatomical labels to each region of the cortical surface (every point in the cortex is identifiable). This procedure is based on probabilistic information estimated from a manually labeled set of images (Fischl et al., 2004).

All the automatic procedures mentioned above were compared with manual procedures, that are known to take a long time to complete (even by trained professionals) and/or give inaccurate results (Fischl and Dale, 2000)(Dale et al., 1999)(Fischl et al., 2004).

Statistical Parametric Mapping

SPM or Statistical Parametric Mapping (www.fil.ion.ucl.ac.uk/spm) is an open source software package used to process and analyse brain imaging data (fMRI, PET, SPECT, EEG and MEG). The software implements the statistic theoretical concepts created by Karl Friston (Friston, 2003). More details about its methods will be given in section 3.2.2.

Conn

Conn is a functional connectivity toolbox (www.nitrc.org/projects/conn) installed within the FSL (Jenkinson et al., 2012) and Matlab environments and it is used to estimate and infer ROI-to-ROI, seed-to-voxel and voxel-to-voxel functional connectivity. It can also compute graph-theory parameters regarding ROI networks.

The analyses performed were based on a model-dependent method. The toolbox provides four connectivity measures: bivariate correlation, semipartial correlation, bivariate regression and multiple regression. In this project the bivariate correlation was used, because it is a measure of the functional connectivity between two areas.

On the other hand the semi-partial correlation is used when studying the contribution of a single ROI in a target area. Bivariate and multiple regression are used when effective connectivity measures are wanted.

This toolbox automatically applies a component-based noise correction method (CompCor) for noise reduction (from both physiological and other sources), removal of movement and temporal covariates, first-level estimation of various functional connectivity MRI measures and second-level random-effect analyses for resting-state and task-related data.

Diffusion Toolkit and TrackVis

Diffusion toolkit (DTK) is a freely available set of tools used for the reconstruction of diffusion imaging data and generation of fiber tracks (Wang et al., 2007). The main workflow performed by DTK includes the reconstruction of the diffusion image volumes to diffusion tensor maps and the creation of whole-brain fiber tracks. For diffusion tensor estimation, it uses linear least-squares fitting method and for DTI fiber tracking, it uses the standard fiber assignment by continuous tracking (FACT) as the default method (Mori et al., 1999).

TrackVis is also a freely available software used to visualize and analyze fiber tracks created from MR images by DTI and other diffusion imaging techniques (Wang and Wedeen, 2010).

3.2 Methods

The sample data was generously provided by the Institute of Child Health (UCL) for use in this project and consists in the collection of anatomic (T1) and functional acquisitions (rs-fMRI) from twenty-two healthy volunteers (both male and female) and structural (DTI) acquisitions from eighteen subjects.

3.2.1 Cortical Thickness and ROI extraction

In order to assess the cortical thickness information and to extract the ROIs for each subject, the structural images (T_1 weighted images, 1 mm^3) were processed by FreeSurfer. A basic explanation of the FreeSurfer procedures was given in section

3.1. The chores for this software are set up by typing the commands in a terminal window. The following command line performs the cortical reconstruction process:

```
recon-all --i T1.mgz --subject subject1 --all
```

where `i` is the argument for the structural image and `subject` is the argument that allows to identify the subject. This process takes about twenty hours to perform (on a standard 8GB RAM desktop), for each subject. After it is finished it's possible to access the white/gray and pial surfaces, an example is given in figure 3.1 on the left.

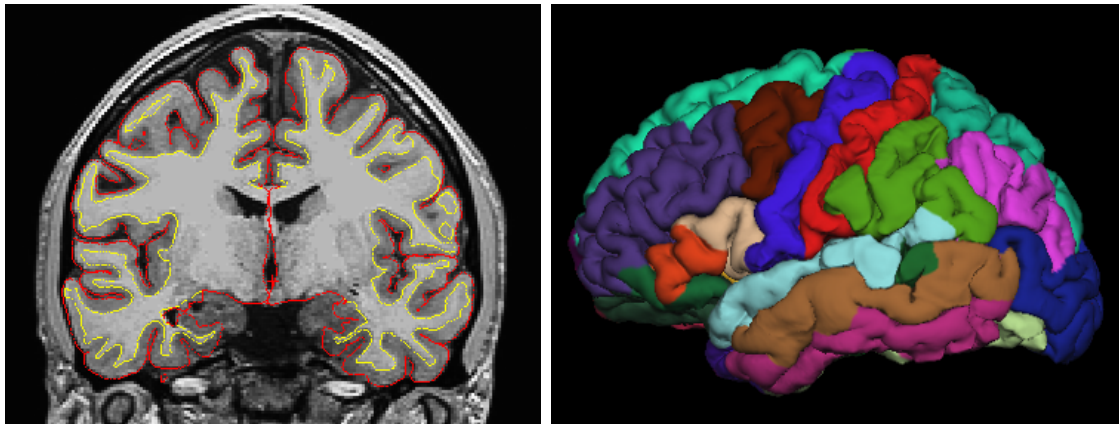


Figure 3.1: Left: White/gray (yellow) and pial (red) surfaces; Right: Cortical surface parcellation of the left hemisphere based on the Desikan-Killiany cortical atlas

The command line used to obtain the cortical thickness measures is the following one:

```
aparcstats2table --hemi lh --subjects subject1 --meas thickness --tablefile  
lh.subject1.corticalthickness.table
```

where `aparcstats2table` is the command itself, the `hemi` argument defines the hemisphere in question, `subjects` identify the chosen subject, `meas thickness` gives the mean thickness for each region in millimetres and `tablefile` is the output argument.

FreeSurfer reconstruction provides two cortical parcellations, one is based on the Desikan-Killiany cortical atlas, which divides the cortex into 68 regions and the other is based on the Destriaux cortical atlas dividing the cortex into 148 regions. The first one defines its' regions from the sulci and the second one from both sulci and gyri.

Ideally, the parcellation scheme should cover the surface of the cortex completely and individual ROIs should not overlap spatially. The atlas used in this project is the Desikan-Killiany, a list of the regions is given with the results in section 4.1 and an image representation is given on figure 3.1 on the right. The parcellation volume is automatically output by FreeSurfer (aparc+aseg.mgz), but before using it, it needs to go through a dilation process:

```
fslmaths originalfile.nii -dilD outputfile.nii
```

where the spatial filtering operation `-dilD` applies a modal dilation of non-zero voxels. The principle objective of this operation is to fill holes within any of the regions by enlarging the boundaries of the non-zero voxels.

The dilated parcellation volume is then registered to the functional image space (described in detail in the next section) and finally each ROI can be extracted into different files:

```
fslmaths dilatedPar.nii -thr 1000.5 -uthr 1001.5 -bin -lh_bankssts.nii
```

Each ROIs is associated with a certain interval of values attributed by FreeSurfer. These values can be accessed on the LUT.txt file output by recon-all process. To isolate a certain ROI from the parcellation file, the code above establishes a lower and upper threshold, resetting the voxels within this interval with the value of one and the ones outside with zero, producing a binary mask.

3.2.2 fMRI preprocessing

In order to infer results from the resting BOLD data, this data needs to be submitted to a certain number of steps, each one of which will attempt to increase the signal to noise ratio by removing data variability. These steps are more or less the same as the ones applied to the “traditional” task-related BOLD fMRI data but of course it will depend on the study case itself.

The first step for this study consisted in deleting the first ten functional images for each subject. This is done because the net magnetization in the beginning of the acquisition hasn’t reached a steady state.

The remaining images were then re-aligned by using a least square approach and rigid body spatial transformations. This step is performed in order to eliminate shifts in the position of the voxels through the images that could result in false-positive activations.

The next step was to coregister the images. A non-rigid registration (nearest neighbor interpolation) is applied to the structural image and the parcellation file (described in detail in the previous section), so they can be in the same space as the functional image. It is always good practice to verify the registration as shown in figure 3.2, where it is possible to check that the images are properly overlaid.

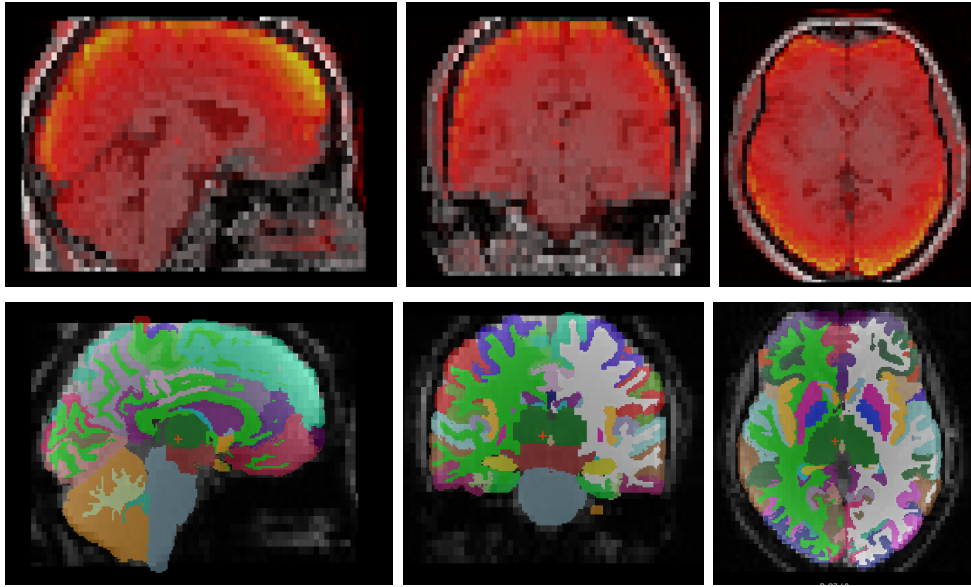


Figure 3.2: Top: Functional images (heat) over the structural images (grayscale); Bottom: parcellation images (LUT) over the functional images (grayscale)

Since the subjects will be studied individually and not as part of a group analysis, the normalization step was skipped. Even more, because the normalization procedure will perform voxel transformations, the cortical volume may change and consequently lead to a loss of information in the data. Overall this step was considered inadvisable for this study.

All these preprocessing steps were performed using SPM (Ashburner et al., 2012).

3.2.3 First-Level Analysis

To perform the analyses using Conn, the user needs the previously preprocessed functional data, one anatomical volume for each subject, the ROIs and the experi-

mental information and covariates.

This project included a total of 22 subjects that will be analysed individually. Each session was performed with a TR of 2.376 seconds, which makes a total running time for 255 images of 605.88 seconds.

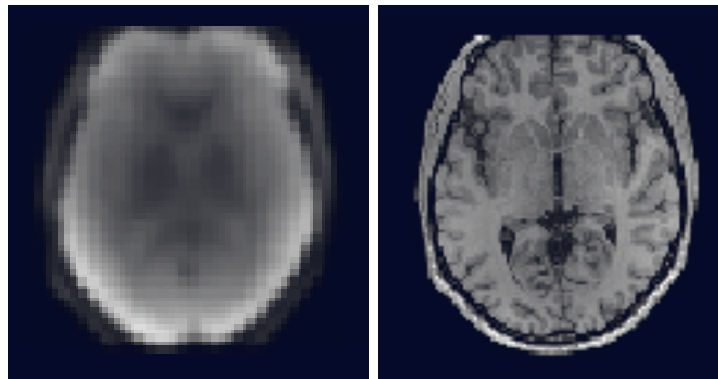


Figure 3.3: Left: rs-fMRI; Right: T1 weighted structural image.

The first step is to load the resting-state functional images and the T1 image for the same subject, figure 3.3 on the left and right, respectively. The ROIs are also imported in this step. All these images are expected to be previously preprocessed and coregistered.

The last file to be imported is the realignment parameters file as a covariate, this will take into account the the subject motion contribution to the BOLD signal and regress it out of the time-series, figure 3.4. In this image, the green line represents the translational movement in the y axis, the red and the blue represent respectively the z and x axes.

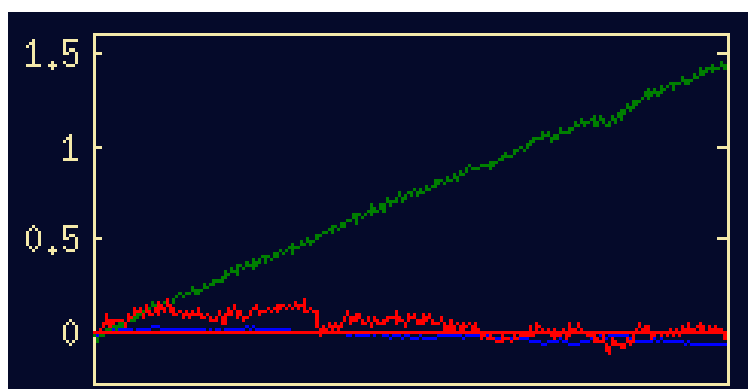


Figure 3.4: Translation movement, the vertical axis is in mm and the horizontal axis represents the scan volume (255 images).

The last thing to do in this step is to define the analyses to be made. For

this project a ROI-to-ROI analyses was performed producing an output file of the confound corrected time-series.

After all this is set up, Conn will perform a pre-analysis that enables the user to preview the results and modify if necessary some of the steps above. Here it is possible to change the band-pass filter definitions. In this study the default values (0.008 - 0.09 Hz) were used.

Figure 3.5 represents a preview of the results for one subject. In this image it is possible to observe the total contribution of the four selected ROIs and it is possible to define a threshold for these results. This way, only voxels that have above a certain r-value will be highlighted.

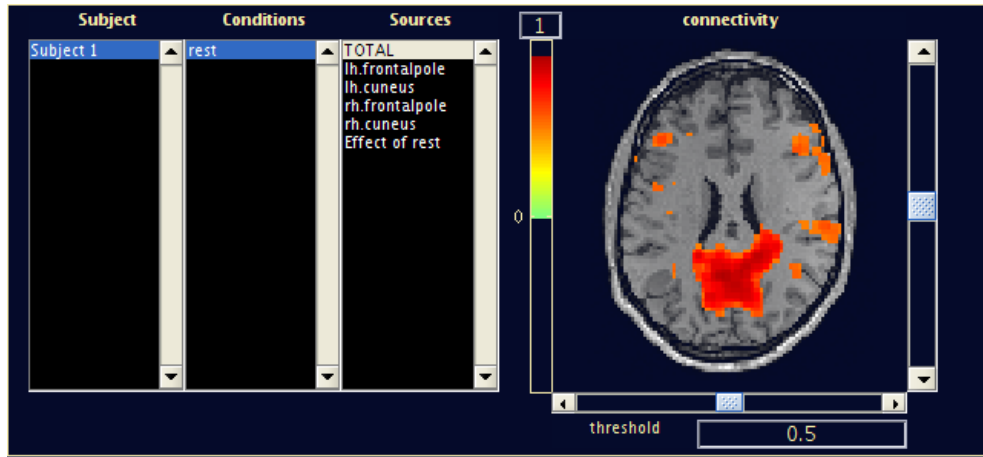


Figure 3.5: Preview results for one subject, including four ROIs.

Finally, statistics are calculated. The first thing Conn computes is the average BOLD time-series for all the voxels within a ROI. The bivariate correlation coefficients (r-values) measure the level of linear association of the time-series between two sources and can be computed for each subject/condition/source. The final output file will contain a matrix Z with the ROI-to-ROI connectivity values, obtained by applying the Fisher transformation to the correlation values (this process is automatically done by Conn). In this project the correlation coefficients (r) will be analysed, in order to do this, the Z -maps were re-converted to correlation maps using Fisher's inverse transform (z -to- r):

$$R = \frac{\exp(2 * Z) - 1}{\exp(2 * Z) + 1} \quad (3.1)$$

This coefficient must be treated with caution, as it varies between -1 and 1, the closer it gets to one of those limits, the stronger the relationship between the two variables, but for example a r-value of 0.50 doesn't mean a 50% relationship between the variables.

3.2.4 Statistical Analysis

The methods used to correlate cortical thickness with functional connectivity will be explained in this section. Part of the analysis was obtained by using the raw values of cortical thickness and correlation coefficients, while the rest were achieved by using processed data.

The raw data analysis consisted in identifying the five highest and lowest correlation coefficients for each subject, determining which ROIs they associated and their thickness and measuring the correlation between these two quantities. The results will be tested by means of a t-test with a 95% confidence interval, the null hypothesis being the non-existence of a relationship between the cortical thickness and the correlation coefficients, that are representing functional connectivity.

From here, two approaches were tested to ensure the validity of the results. Because there is still a lot of contradiction regarding the accurate meaning of a negative correlation, two designs were applied to the original data, one that includes the anti-correlations and one that didn't. For the data that included all values, every entry of the matrices were squared (because of mean purposes) and then all the contributions for each region were summed (sum of all the values in each line), so that in the end the data is one column per subject, with only one value per ROI. For the other data, a threshold was applied to the matrices in order to delete every value below zero, and again every value for each line was summed. This summed value represents the node strength in graph analysis.

At this point the data was made up of three tables, two with values that represent functional connectivity and one with the cortical thickness values. All of them are 22x68, subjects and ROIs respectively. This data can be plotted either by subject or

by ROI, but doing it for each one would provide too numerous results and wouldn't help that much with the analysis. The solution for this was to calculate the means amongst the subjects or ROIs for separate studies. When the mean amongst the subjects was calculated the ROIs worked as a confounding variable (and vice-versa), that needs to be eliminated, by means of a normalization.

Because stronger correlations are more reliable, as weak links may stand for spurious connections, an absolute threshold was applied to the data. The threshold values are regularly determined in an arbitrary way and networks should ideally be characterized across a broad range of thresholds. For this study, the chosen thresholds were 0.2, 0.4, 0.6 and 0.8, when using only the positive correlations, and adding the symmetric thresholds when using the whole data.

3.2.5 Graph Theory Analysis

The matrices submitted to this analysis are binary and undirected, and because the more specialized applications of graph theory that include negative links have not been yet widely applied in neuroscience, only positive correlation matrices were used for the analysis.

For this project, only the core measures of graph theory were considered. These include the degree k , the clustering coefficient and the mean minimum path length. The clustering coefficient $0 < C < 1$ is a ratio that characterizes the local structure, by defining the proportion of possible connections that actually exist between the nearest neighbours of a node. The minimum path length is the number of edges that composes the shortest path between any pair of nodes and the mean minimum path length L is the average of the $n - 1$ minimum path lengths between a certain node and all the other nodes in the network. It works as a global characteristic and indicates how well integrated a graph is and if the information is easily transported within the network. The averaged values of these quantities over nodes are the network means K_{net} and C_{net} and the characteristic path length L_{net} . The hubs of a networks are determined by the smallest values of L or the largest values of K .

These measures were obtained for three different correlation matrices, the original

one without the negative correlation values, and the other too will be submitted to a threshold of 0.2 and 0.4. The principle vantage of applying a threshold is the elimination of weaker connections that have more probability of being data noise. Nevertheless, the small-world properties can only be estimated if $k_{net} > \log(n)$, which can not be achieved if the threshold is too high. These two thresholds were chosen for this project because the correlation matrix thresholded by 0.6 produced a $k_{net} = 2$, which is lower than the $\log(68) = 4.220$. On the other hand, the non thresholded, and thresholded at 0.2 and 0.4 produced $k_{net} = 46$, $k_{net} = 25$ and $k_{net} = 9$, respectively.

In order to determinate the small-world properties for this data, the characteristic path length and the clustering coefficient were compared to the ones estimated using random networks. These random networks have to have the same number of nodes and the mean degree $k_{rand} > \log(n)$.

Usually, in a small-world network, there are certain expected values, such as $\gamma = C_{net}/C_{rand} > 1$ and $\lambda = L_{net}/L_{rand} \simeq 1$. To sum it up, a scalar summary of small-worldliness can be determined by the ratio $\sigma = \gamma/\lambda$, which should be > 1 (Achard et al., 2006).

3.2.6 Structural Analysis

The first step taken in the statistical analysis part of this project was the creation of the fiber tracks, for each subject, using DTK. All fiber tracks files were then checked with TrackVis.

The second step consisted in the registration of the FreeSurfer parcellation file to the DTI space, using FSL. The chosen registration procedure included:

fslreorient2std originalImage.nii reorientedImage.nii

where fslreorient2std applies rotations to the images in order to match their orientation with the standard template images (MNI152). This reorientation was applied to the T1 images and the parcellation files. The next step was:

bet originalImage.nii stripedImage.nii

where the brain extraction tool (BET) deletes non-brain tissue from an image of the

whole head (Smith, 2002). This extraction was applied to both T1 and DTI data. The real registration steps start at this point with:

```
flirt -i dti.nii -ref T1.nii -omat flirt.mat
```

where `flirt` is a tool to perform linear (affine) brain image registration and `i`, `ref` and `omat` represent the input, reference and the output for the ascii transformation matrix, respectively. Followed up by:

```
fnirt --ref=T1.nii --in=dti.nii --aff=flirt.mat  
--config=FA_2_FMRIB58_1mm.cnf --cout=transformation
```

where `fnirt` performs non-linear registration and `ref`, `in`, `aff` and `cout` represent the reference, input, transformation and output files, respectively. The configuration file `FA_2_FMRIB58_1mm.cnf` is a text file that contains many of the parameters that FNIRT takes (and values for them). The next step was:

```
invwarp -w transformation.nii -o invTransformation.nii -r dti.nii
```

where `invwarp` is used to reverse a non-linear mapping, `w` is the original transformation `o` the inverted transformation output and `r` the new reference image. The final step was:

```
applywarp --ref=dti.nii --in=parcellation.nii --out=warpedParcelation.nii  
--warp=invTransformation.nii --interp=nn
```

where `applywarp` applies the transformation to a given file, `ref`, `in`, `out` and `warp` represent the reference, input, output and transformation files, respectively, and `interp` is used in order to implement the nearest neighbor interpolation.

With the registration completed, it is possible to calculate the number of fibers between pairs of ROIs and computing them in a structural connectivity matrix (s-CM), using the software developed by Ribeiro et al., 2013.

This procedure resulted in eighteen 68x68 matrices in which the entries represent the number of fibers. For a simpler analysis all entries were summed for each ROI resulting in one final matrix of 18x68, subjects and ROIs respectively. The means

amongst subjects and ROIs were calculated and plotted against the mean cortical thickness. A correlation coefficient was also calculated between these two variables, and afterwards tested with a 95% confidence interval t-test, the null hypothesis being the non-existence of a relationship between them.

Chapter 4

Results and Discussion

The results obtained in this thesis will be described and discussed in this chapter.

4.1 Cortical Thickness

The table 4.1 shows the measures of the cortical thickness for 68 regions of interest for both right and left hemispheres, for three subjects (the results for all twenty-two subjects are given in appendix A). These results were obtained by following the procedure explained in section 3.2.1.

Although some ROIs cross two or more lobar boundaries, most of them can be mapped to the lobes:

Frontal

- Superior frontal
- Rostral and Caudal Middle Frontal
- Pars Opercularis, Triangularis and Orbitalis
- Lateral and Medial Orbitofrontal
- Precentral
- Paracentral
- Frontal pole

Parietal

- Superior Parietal
- Inferior Parietal
- Supramarginal
- Postcentral
- Precuneus

Temporal

- Superior, Middle and Inferior temporal
- Banks of the Superior Temporal Sulcus
- Fusiform
- Transverse temporal
- Entorhinal
- Temporal pole
- Prahippocampal

Occipital

- Lateral Occipital
- Lingual
- Cuneus
- Pericalcarine

The only analyses applied to these results were the calculation of the mean thickness 2.7 mm, the maximum 4.3 and the minimum 1.6 mm which all fall into agreement with the information given in (Gazzaniga et al., 2008), that states that

Table 4.1: Cortical thickness (mm) of 68 ROIs (left and right hemispheres) for three subjects

| ROI | Subject 1 | | Subject 2 | | Subject 3 | |
|----------------------------|-----------|-----|-----------|-----|-----------|-----|
| | LH | RH | LH | RH | LH | RH |
| Bankssts | 1.9 | 2.7 | 2.6 | 2.9 | 1.9 | 2.7 |
| Caudal Anterior Cingulate | 2.5 | 2.4 | 2.9 | 2.6 | 2.6 | 2.4 |
| Caudal Middle Frontal | 2.7 | 2.9 | 2.7 | 2.7 | 2.8 | 2.9 |
| Cuneus | 1.9 | 2.0 | 1.9 | 1.8 | 2.0 | 1.9 |
| Entorhinal | 2.9 | 3.1 | 3.2 | 3.4 | 3.4 | 3.0 |
| Fusiform | 3.0 | 2.8 | 2.9 | 3.0 | 2.8 | 2.8 |
| Inferior Parietal | 2.7 | 2.7 | 2.6 | 2.7 | 2.6 | 2.7 |
| Inferior Temporal | 2.5 | 2.9 | 2.7 | 3.0 | 2.8 | 3.0 |
| Isthmus Cingulate | 2.5 | 2.3 | 2.6 | 2.3 | 2.5 | 2.5 |
| Lateral Occipital | 2.2 | 2.4 | 2.3 | 2.3 | 2.2 | 2.3 |
| Lateral Orbito Frontal | 2.9 | 2.9 | 2.8 | 2.9 | 2.9 | 2.8 |
| Lingual | 2.1 | 2.2 | 2.0 | 2.1 | 2.2 | 2.2 |
| Medial Orbito Frontal | 2.9 | 2.6 | 2.6 | 2.7 | 2.6 | 2.6 |
| Middle Temporal | 2.2 | 2.8 | 2.6 | 3.0 | 2.6 | 3.1 |
| Parahippocampal | 3.0 | 2.8 | 3.0 | 2.8 | 2.8 | 2.5 |
| Paracentral | 2.5 | 2.6 | 2.4 | 2.4 | 2.3 | 2.4 |
| Parsopercularis | 2.9 | 2.9 | 2.5 | 2.8 | 2.7 | 2.9 |
| Parsorbitalis | 3.0 | 2.8 | 3.0 | 3.0 | 3.2 | 3.1 |
| Parstriangularis | 2.9 | 2.7 | 2.6 | 2.8 | 2.8 | 2.7 |
| Pericalcarine | 1.8 | 1.7 | 1.6 | 1.7 | 2.1 | 2.1 |
| Postcentral | 2.0 | 2.2 | 2.3 | 2.3 | 2.2 | 2.2 |
| Posterior cingulate | 2.7 | 2.5 | 2.5 | 2.5 | 2.5 | 2.6 |
| Precentral | 2.4 | 2.5 | 2.4 | 2.5 | 2.6 | 2.6 |
| Precuneus | 2.6 | 2.5 | 2.6 | 2.6 | 2.6 | 2.6 |
| Rostral Anterior Cingulate | 3.0 | 3.0 | 3.1 | 3.0 | 2.6 | 2.7 |
| Rostral Middle Frontal | 2.6 | 2.7 | 2.6 | 2.7 | 2.7 | 2.7 |
| Superior Frontal | 3.0 | 2.9 | 2.9 | 3.0 | 3.1 | 3.1 |
| Superior Parietal | 2.5 | 2.6 | 2.4 | 2.5 | 2.5 | 2.5 |
| Superior Temporal | 2.6 | 2.9 | 2.6 | 2.8 | 2.5 | 2.8 |
| Supramarginal | 2.2 | 2.7 | 2.3 | 2.7 | 2.2 | 2.8 |
| Frontal Pole | 2.9 | 2.9 | 3.1 | 2.8 | 3.2 | 3.1 |
| Temporal Pole | 4.2 | 4.2 | 3.9 | 4.0 | 3.7 | 4.3 |
| Transverse Temporal | 2.6 | 2.5 | 2.5 | 2.4 | 2.7 | 2.7 |
| Insula | 3.3 | 3.5 | 3.0 | 3.3 | 3.0 | 3.2 |

the human cerebral cortex thickness averages around 3 mm and varies between 1.5 and 4.5 mm.

4.2 First-Level Analysis

As it was explained in section 3.2.2, the final output from Conn Toolbox is a Z-map for each of the subjects. These maps are then converted to correlation coefficients maps by the use of the Fisher's Inverse Transform (equation 3.1). Figure 4.1 shows these connectivity maps for the first subject (the maps for the remaining subjects are provided in appendix B).

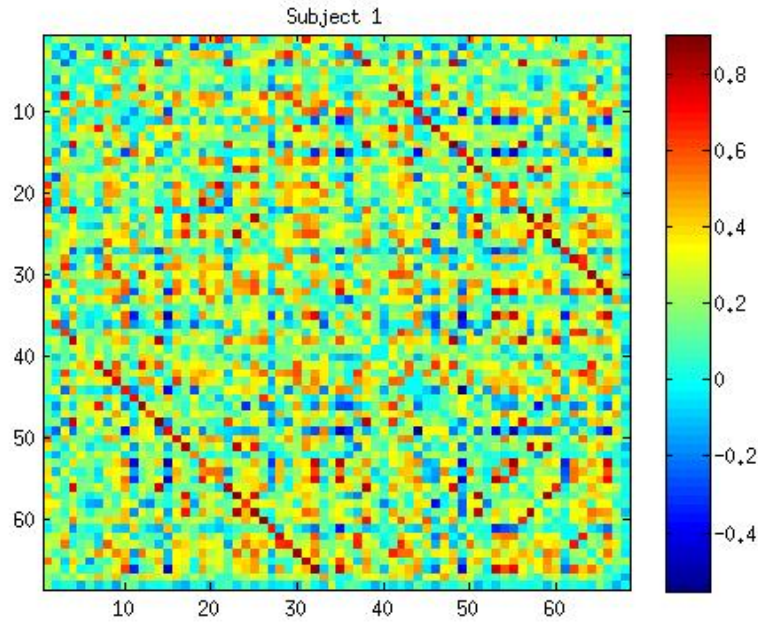


Figure 4.1: Correlation coefficient map for subject one.

In this matrix rows and columns represent the ROIs, while the matrix entries represent the linear Pearson correlation coefficients between the time courses of each pair of ROIs. The order of the nodes does not influence the computation of network measures.

Although not much information can be extracted from these matrices, in all of them it's easy to distinguish two dark red diagonals, which represent the strong connections that exist between symmetric areas of the brain.

Although these correlation coefficients only express the degree to which a region is connected to another functionally, they were used in the rest of the analysis as a measure of functional connectivity of the brain.

In order to better understand the time-series obtained from rs-fMRI, the maximum

and minimum correlation coefficients were identified for subject number one. The highest positive correlation coefficient had a value of $r = 0.9021$ and the lowest negative $r = -0.5521$. The positive value corresponds to the correlation between the time-series from the middle temporal ROI, for both hemispheres (figure 4.2 on top). This symmetry phenomenon was not observed for the anti-correlation value, that corresponds to the correlation between the time-series from the parahippocampal and lateral occipital ROIs, both from the right hemisphere (figure 4.2 at the bottom).

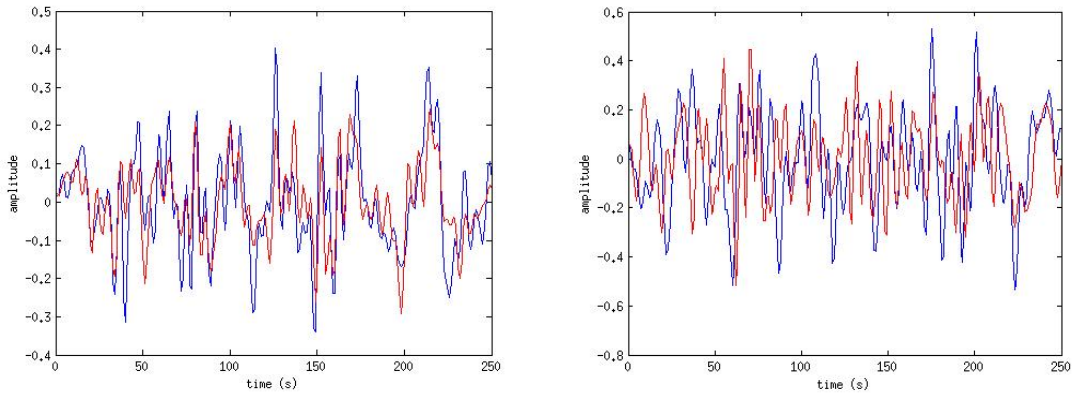


Figure 4.2: Left: Comparison of the time-series between the middle temporal ROI of the left (blue) and right (red) hemispheres, for subject one; Right: Comparison of the time-series between the lateral occipital (blue) and parahippocampal (red) ROIs, of the right hemisphere, for subject one

4.3 Statistical Analysis

The results for the main objective of this project (correlating cortical thickness with functional connectivity) will be detailed in this section.

The results obtained from using the raw data showed that the highest correlation coefficients were mainly associating with symmetric regions of the brain, supporting, this way, the observation made in the previous section. As shown below, the five lowest correlation coefficients didn't present any kind of significant results, and for this reason this part of the analysis was discarded.

The plots presented in figure 4.3 show, in the right and left respectively, the relation between the cortical thickness and the maximum correlation coefficient for every subject and the relation between cortical thickness and the five highest values

of the correlation coefficients again for every subject. The value of cortical thickness here is the mean between the two regions correlated. Each plot contains also a linear regression line and the Pearson correlation coefficient for these two quantities.

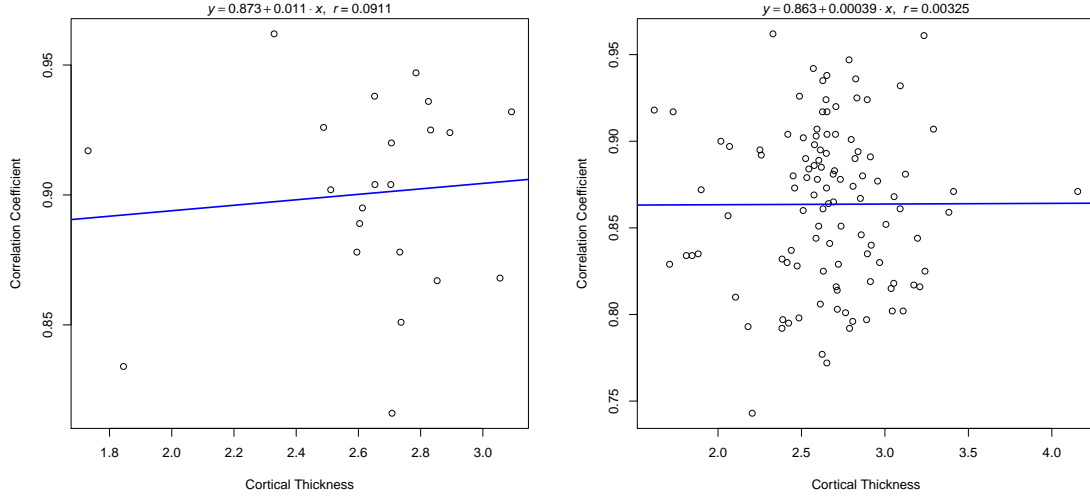


Figure 4.3: Left: relation between the cortical thickness and the maximum correlation coefficient for every subject and Right: relation between cortical thickness and the five highest values of the correlation coefficients for every subject.

What can be observed here is that the Pearson's $r = 0.091$ and $r = 0.003$ indicate a weak positive relationship, and that there is a significant decrease on the correlation when the size of the data is increased. The significance of these values was obtained by doing a t-test with a 95% confidence interval, the null hypothesis being the non-existence of a relationship. The results for the data plotted on left of figure 4.3 were $t = 0.409$ and $p = 0.687$ and because t doesn't equal or exceed $t(20) = 2.086$, there is evidence to support the null hypothesis, in other words, it's highly possible that there is no relation between functional connectivity and cortical thickness, according to this data. The results for the data on the right plot were fairly similar, with a $t = 0.034$ and $p = 0.973$ against a $t(108) = 1.982$.

Still using this data, from the five highest values of the correlation coefficients for every subject, the three ROIs that have the highest degree of occurrence were drawn out. They were the Rostral Middle Frontal, Rostral Anterior Cingulate and the Precentral. The values of correlation coefficient and cortical thickness were plotted for each region, as showed in figure 4.4.

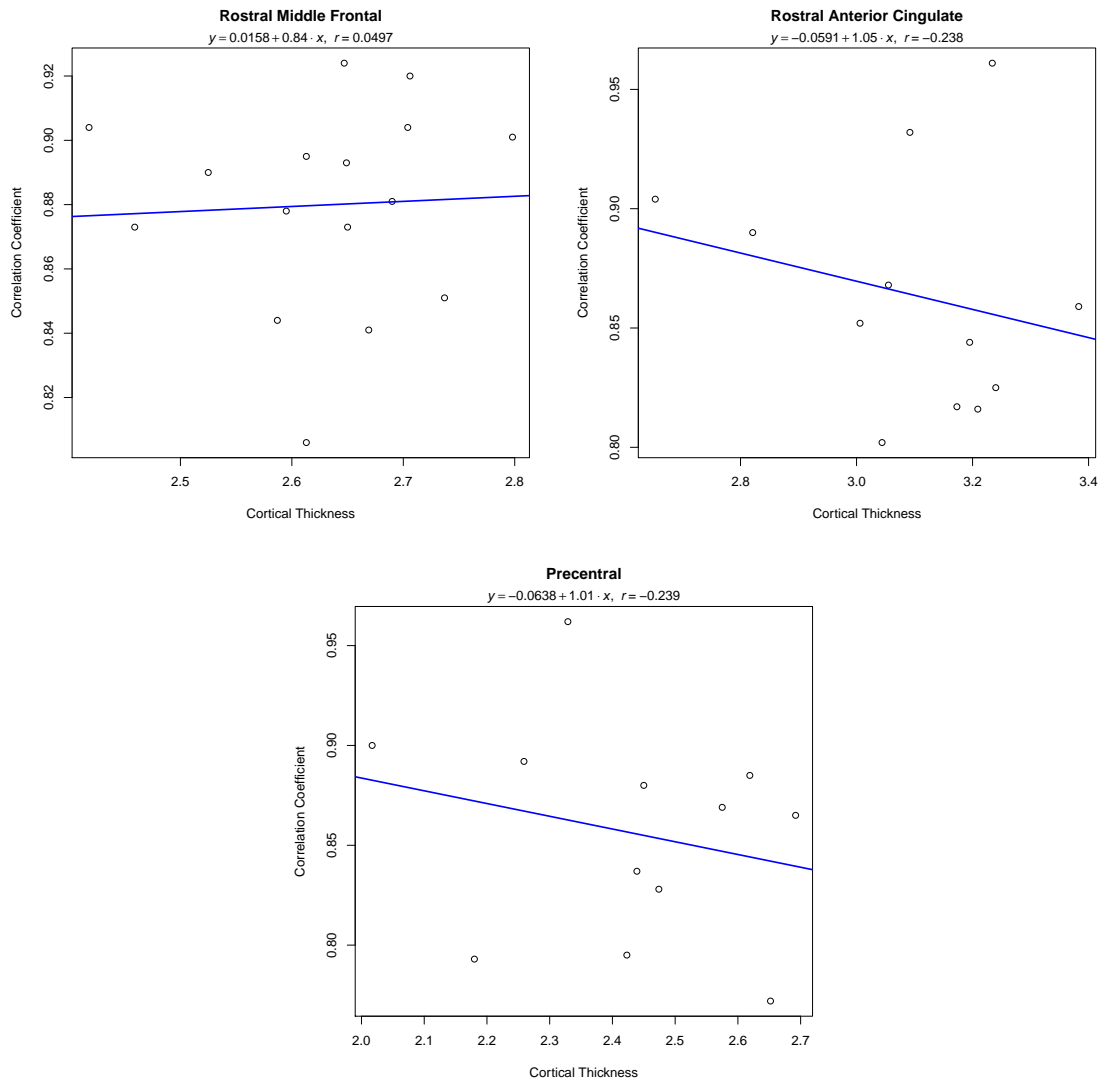


Figure 4.4: Relation between the cortical thickness correlation coefficient for the: (Upper Left) Rostral Middle Frontal; (Upper Right) Rostral Anterior Cingulate; and (Bottom) Precentral.

The biggest difference that can be seen in these plots is the negative correlation for the Rostral Anterior Cingulate and Precentral ROIs. The results for the t-test applied to this data were: for the rostral middle frontal a $r = 0.050$ ($t = 0.186$; $p = 0.855$); for the rostral anterior cingulate a $r = -0.238$ ($t = -0.775$; $p = 0.456$); and for the precentral a $r = -0.239$ ($t = -0.779$; $p = 0.454$). These results support once again the hypothesis of a non existent relation between cortical thickness and functional connectivity.

The results presented from now on, were obtained after doing calculations on

the original data. The first step was to take the matrices shown in figure 4.1 and appendix B and for the study case that includes all values, every entry of the matrices was squared (for mean purposes) and for the case that includes only the positive correlations only the zero threshold was applied.

The second step, common to both studies, consisted in summing all the contributions for each region and divide by the number of regions connected to it. The outcome is a mean correlation value per ROI and per subject.

At this point the data is made up by three tables, two with values that represent functional connectivity and one with the cortical thickness values. All of them are 22x68, subjects and ROIs respectively. The means for these tables were calculated both amongst the subjects and ROIs.

Figure 4.5 shows the results for the mean of all regions per subject (twenty-two data points). In order to do this correctly, the effect that the ROIs produce on the data needs to be regressed out. In other words, the mean for each region should be zero and the standard deviation unitary.

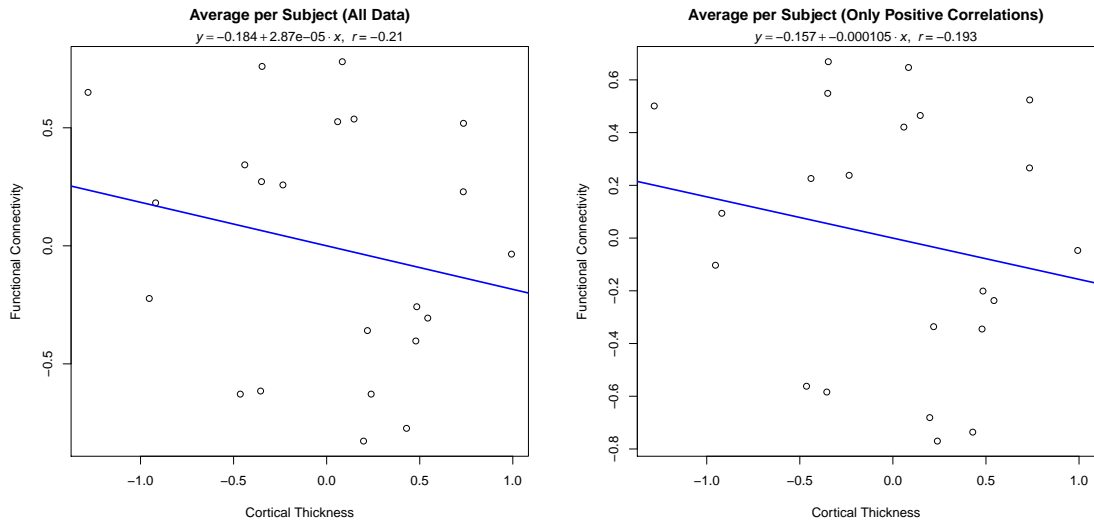


Figure 4.5: Average correlation coefficients and cortical thickness by subject for: (Left) all data; (Right) only positive correlations.

Again, the correlation coefficient for these results indicates a negative relationship, but the results given by the t-test presented for all the data a $r = -0.210$ ($t = -0.958$; $p = 0.349$) a for the data with only the positive correlations a $r = -0.193$ ($t = -0.880$; $p = 0.389$), don't support the hypothesis that there exists any significant association.

The correlation coefficient decreases from the left plot to the right one, but it doesn't really help to take conclusions about the real effect caused by negative correlations.

Figure 4.6 shows the results for the mean of all subjects per region (sixty-eight data points). For this case, the effect that the subjects produce on the data, needs to be regressed out.

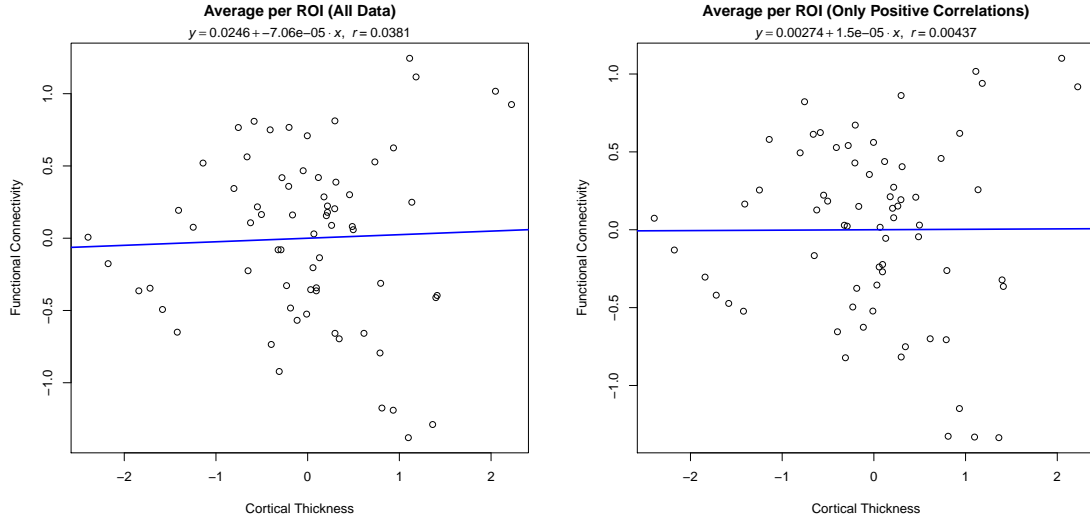


Figure 4.6: Average correlation coefficients and cortical thickness by ROI for: (Left) all data; (Right) only positive correlations.

Although the correlation coefficient is positive in these results, it turns out considerably smaller when comparing with the results of figure 4.5. It is therefore not surprising that the t-test for these results support the non-existence of a relationship between these two quantities. The produced t-test values were for all the data a $r = 0.038$ ($t = 0.309$; $p = 0.758$) and for the positive correlations only a $r = 0.004$ ($t = 0.036$; $p = 0.972$).

The graphical results for the thresholded matrices can be viewed in appendix C, and here is presented a summary table with the correlation values between cortical thickness and functional connectivity for all study cases. Even though there is no statistical significance associated with these results, some particularities can be observed.

As it can be seen, there is no pattern that determines the correlation values for all studies. The values given by subject show a negative correlation that suggests that

Table 4.2: Correlation values between cortical thickness and functional connectivity for all study cases.

| Threshold | By Subject | | By ROI | |
|-----------|------------|-----------------------|----------|-----------------------|
| | All Data | Positive Correlations | All Data | Positive Correlations |
| 0 | -0.238 | -0.193 | 0.038 | 0.004 |
| 0.2 | -0.210 | -0.157 | 0.024 | 0 |
| 0.4 | -0.237 | -0.177 | 0.150 | -0.170 |
| 0.6 | -0.0201 | -0.198 | -0.146 | -0.152 |
| 0.8 | -0.190 | -0.262 | 0.068 | 0.069 |

a person with a thinner cortex will present a higher functional connectivity, however the t-test performed for these values, secure the acceptance of the null hypothesis of a non-existent relationship between these two quantities. Also there seems to be no difference in calculating this correlation coefficient with or without applying a threshold to the data.

The values given by ROI seem even more random, but overall the correlation enhances from a zero to a 0.8 threshold, although it doesn't lead to any conclusions.

4.4 Graph Theory Analysis

All the results presented in this section were estimated from binary and undirected correlation coefficient matrices that include only positive correlations.

The core measures of graph theory considered for this project are degree k , the clustering coefficient C and the mean minimum path length L . All the results are given in table 4.3 for all the left hemisphere regions, for the three different thresholds. The results for the right hemisphere regions are given in table 4.4. The hubs of a networks are determined by the smallest values of L or the largest values of K , and this was observed for more or less half of the regions. The degree was obtained by summing all the connections per matrix and averaging over subjects. The clustering coefficient and the mean minimum path length were obtained using the brain connectivity toolbox `clustering_coef_bu` and `distance_bin` functions (Rubinov and Sporns, 2010) and averaging over subjects.

The averaged degree over nodes for the three different thresholds are $K_{net} = 46$, $K_{net0.2} = 25$ and $K_{net0.4} = 9$, respectively. These values guarantee the significant

Table 4.3: Cortical thickness (mm), degree (K), clustering coefficient (C) and characteristic path length (L), for each region of the left hemisphere, estimated from three correlation matrices, differing only in the threshold used.

| | | No Threshold | | | Threshold 0.2 | | | Threshold 0.4 | | |
|----------------|---------|--------------|-------|-------|---------------|-------|-------|---------------|-------|-------|
| ROI | Co. Th. | K | C | L | K | C | L | K | C | L |
| Bankssts | 2.4 | 46 | 0.782 | 1.320 | 24 | 0.642 | 1.719 | 8 | 0.519 | 2.393 |
| Cau. Ant. Cin. | 2.7 | 45 | 0.785 | 1.334 | 22 | 0.660 | 1.768 | 7 | 0.513 | 2.859 |
| Cau. Mid. Fro. | 2.7 | 48 | 0.784 | 1.285 | 27 | 0.624 | 1.677 | 10 | 0.565 | 2.451 |
| Cuneus | 1.9 | 44 | 0.767 | 1.350 | 22 | 0.590 | 1.806 | 8 | 0.569 | 3.075 |
| Entorhinal | 3.1 | 45 | 0.768 | 1.336 | 16 | 0.639 | 1.927 | 3 | 0.377 | 1.723 |
| Fusiform | 2.8 | 41 | 0.773 | 1.390 | 17 | 0.653 | 1.885 | 5 | 0.399 | 2.829 |
| Inf. Par. | 2.6 | 42 | 0.773 | 1.381 | 21 | 0.610 | 1.828 | 7 | 0.507 | 2.398 |
| Inf. Tem. | 2.7 | 49 | 0.779 | 1.275 | 27 | 0.624 | 1.669 | 11 | 0.521 | 2.398 |
| Ist. Cin. | 2.5 | 47 | 0.770 | 1.294 | 26 | 0.564 | 1.660 | 9 | 0.447 | 2.674 |
| Lat. Occ. | 2.2 | 46 | 0.792 | 1.315 | 28 | 0.663 | 1.687 | 12 | 0.527 | 2.396 |
| Lat. Orb. Fro. | 2.8 | 46 | 0.765 | 1.321 | 23 | 0.611 | 1.754 | 9 | 0.553 | 2.740 |
| Lingual | 2.0 | 46 | 0.760 | 1.311 | 22 | 0.589 | 1.739 | 6 | 0.442 | 3.026 |
| Med. Orb. Fro. | 2.7 | 47 | 0.775 | 1.292 | 25 | 0.594 | 1.717 | 9 | 0.533 | 2.585 |
| Mid. Tem. | 2.5 | 36 | 0.752 | 1.457 | 16 | 0.605 | 2.045 | 6 | 0.529 | 3.129 |
| Parahippoca. | 2.8 | 44 | 0.789 | 1.346 | 23 | 0.637 | 1.752 | 9 | 0.528 | 2.830 |
| Paracentral | 2.3 | 49 | 0.784 | 1.269 | 31 | 0.594 | 1.603 | 14 | 0.481 | 2.396 |
| Parsoper. | 2.7 | 50 | 0.769 | 1.249 | 27 | 0.702 | 1.687 | 10 | 0.709 | 2.700 |
| Parsorb. | 3.0 | 44 | 0.759 | 1.346 | 17 | 0.588 | 1.919 | 3 | 0.394 | 2.162 |
| Parstriar. | 2.7 | 47 | 0.795 | 1.301 | 28 | 0.615 | 1.662 | 11 | 0.555 | 2.440 |
| Pericalcarine | 1.7 | 43 | 0.788 | 1.362 | 23 | 0.635 | 1.767 | 8 | 0.515 | 2.577 |
| Postcentral | 2.1 | 47 | 0.790 | 1.292 | 26 | 0.647 | 1.706 | 10 | 0.567 | 2.505 |
| Pos. Cin. | 2.6 | 39 | 0.764 | 1.417 | 17 | 0.669 | 1.961 | 6 | 0.734 | 3.400 |
| Precentral | 2.4 | 50 | 0.788 | 1.261 | 28 | 0.669 | 1.653 | 12 | 0.670 | 2.566 |
| Precuneus | 2.6 | 53 | 0.761 | 1.215 | 32 | 0.610 | 1.592 | 13 | 0.548 | 2.428 |
| Ros. Ant. Cin. | 3.1 | 50 | 0.789 | 1.252 | 31 | 0.643 | 1.620 | 14 | 0.623 | 2.499 |
| Ros. Mid. Fro. | 2.6 | 50 | 0.749 | 1.261 | 27 | 0.559 | 1.641 | 11 | 0.558 | 2.581 |
| Sup. Fro. | 3.0 | 44 | 0.791 | 1.339 | 21 | 0.629 | 1.770 | 7 | 0.475 | 2.623 |
| Sup. Par. | 2.4 | 51 | 0.764 | 1.246 | 28 | 0.598 | 1.619 | 11 | 0.454 | 2.412 |
| Sup. Tem. | 2.6 | 54 | 0.755 | 1.199 | 35 | 0.553 | 1.528 | 14 | 0.440 | 2.358 |
| Supramar. | 2.4 | 51 | 0.748 | 1.236 | 29 | 0.573 | 1.607 | 10 | 0.471 | 2.581 |
| Fro. Pole | 3.1 | 49 | 0.760 | 1.273 | 28 | 0.616 | 1.663 | 12 | 0.527 | 2.493 |
| Temp. Pole | 3.6 | 48 | 0.795 | 1.277 | 31 | 0.620 | 1.601 | 15 | 0.495 | 2.292 |
| Trans. Temp. | 2.5 | 44 | 0.783 | 1.341 | 20 | 0.631 | 1.823 | 5 | 0.320 | 2.339 |
| Insula | 3.2 | 51 | 0.759 | 1.245 | 24 | 0.651 | 1.725 | 9 | 0.592 | 2.491 |

estimation of the small-world properties, because they all respect $k_{net} > \log(n) = 4.220$. Three random binary undirected matrices were created to match the number of nodes, mean degree, and degree distribution in order to estimate the small-world

Table 4.4: Cortical thickness (mm), degree (K), clustering coefficient (C) and characteristic path length (L), for each region of the right hemisphere, estimated from three correlation matrices, differing only in the threshold used.

| | | No Threshold | | | Threshold 0.2 | | | Threshold 0.4 | | |
|----------------|---------|--------------|-------|-------|---------------|-------|-------|---------------|-------|-------|
| ROI | Co. Th. | K | C | L | K | C | L | K | C | L |
| Bankssts | 2.7 | 47 | 0.791 | 1.295 | 24 | 0.668 | 1.738 | 8 | 0.678 | 2.676 |
| Cau. Ant. Cin. | 2.7 | 46 | 0.776 | 1.315 | 25 | 0.652 | 1.718 | 9 | 0.520 | 2.638 |
| Cau. Mid. Fro. | 2.8 | 48 | 0.773 | 1.277 | 27 | 0.616 | 1.652 | 10 | 0.550 | 2.415 |
| Cuneus | 2.0 | 39 | 0.762 | 1.417 | 18 | 0.618 | 1.875 | 6 | 0.564 | 2.755 |
| Entorhinal | 3.2 | 45 | 0.768 | 1.326 | 16 | 0.665 | 1.948 | 4 | 0.379 | 1.577 |
| Fusiform | 2.8 | 41 | 0.769 | 1.395 | 17 | 0.665 | 1.906 | 5 | 0.503 | 2.773 |
| Inf. Par. | 2.7 | 45 | 0.764 | 1.332 | 23 | 0.614 | 1.789 | 7 | 0.458 | 2.339 |
| Inf. Tem. | 2.9 | 48 | 0.780 | 1.279 | 28 | 0.632 | 1.638 | 12 | 0.447 | 2.304 |
| Ist. Cin. | 2.5 | 50 | 0.752 | 1.257 | 29 | 0.556 | 1.623 | 9 | 0.433 | 2.548 |
| Lat. Occ. | 2.3 | 45 | 0.790 | 1.334 | 25 | 0.684 | 1.712 | 12 | 0.589 | 2.489 |
| Lat. Orb. Fro. | 2.8 | 45 | 0.765 | 1.324 | 23 | 0.619 | 1.726 | 8 | 0.624 | 2.742 |
| Lingual | 2.1 | 44 | 0.763 | 1.341 | 21 | 0.593 | 1.777 | 6 | 0.390 | 2.855 |
| Med. Orb. Fro. | 2.7 | 46 | 0.773 | 1.310 | 22 | 0.631 | 1.789 | 8 | 0.557 | 2.700 |
| Mid. Tem. | 2.9 | 36 | 0.763 | 1.467 | 15 | 0.630 | 2.044 | 6 | 0.457 | 3.214 |
| Parahippoca. | 2.7 | 43 | 0.792 | 1.351 | 23 | 0.665 | 1.754 | 10 | 0.523 | 2.776 |
| Paracentral | 2.4 | 50 | 0.779 | 1.248 | 32 | 0.587 | 1.587 | 13 | 0.476 | 2.349 |
| Parsoper. | 2.8 | 50 | 0.775 | 1.252 | 27 | 0.685 | 1.665 | 11 | 0.674 | 2.585 |
| Parsorb. | 3.0 | 43 | 0.756 | 1.355 | 16 | 0.668 | 1.983 | 3 | 0.302 | 2.105 |
| Parstriar. | 2.8 | 46 | 0.800 | 1.321 | 26 | 0.658 | 1.694 | 11 | 0.567 | 2.463 |
| Pericalcarine | 1.8 | 45 | 0.790 | 1.324 | 23 | 0.663 | 1.765 | 9 | 0.553 | 2.471 |
| Postcentral | 2.1 | 46 | 0.802 | 1.308 | 27 | 0.636 | 1.674 | 9 | 0.600 | 2.534 |
| Pos. Cin. | 2.6 | 38 | 0.760 | 1.427 | 17 | 0.683 | 1.984 | 6 | 0.697 | 3.140 |
| Precentral | 2.5 | 48 | 0.784 | 1.286 | 27 | 0.705 | 1.713 | 11 | 0.698 | 2.626 |
| Precuneus | 2.5 | 49 | 0.782 | 1.273 | 30 | 0.625 | 1.622 | 12 | 0.531 | 2.441 |
| Ros. Ant. Cin. | 3.1 | 50 | 0.792 | 1.253 | 31 | 0.644 | 1.608 | 14 | 0.612 | 2.472 |
| Ros. Mid. Fro. | 2.6 | 48 | 0.763 | 1.284 | 28 | 0.580 | 1.642 | 11 | 0.528 | 2.467 |
| Sup. Fro. | 3.0 | 44 | 0.774 | 1.347 | 19 | 0.644 | 1.828 | 5 | 0.526 | 2.918 |
| Sup. Par. | 2.4 | 48 | 0.773 | 1.286 | 27 | 0.613 | 1.645 | 10 | 0.478 | 2.393 |
| Sup. Tem. | 2.8 | 52 | 0.770 | 1.223 | 34 | 0.573 | 1.561 | 15 | 0.425 | 2.265 |
| Supramar. | 2.6 | 49 | 0.757 | 1.273 | 28 | 0.574 | 1.645 | 10 | 0.476 | 2.694 |
| Fro. Pole | 3.0 | 49 | 0.777 | 1.265 | 29 | 0.622 | 1.637 | 14 | 0.541 | 2.491 |
| Temp. Pole | 3.5 | 46 | 0.812 | 1.318 | 30 | 0.651 | 1.616 | 15 | 0.485 | 2.304 |
| Trans. Temp. | 2.5 | 46 | 0.779 | 1.313 | 22 | 0.610 | 1.782 | 5 | 0.420 | 2.612 |
| Insula | 3.2 | 48 | 0.760 | 1.281 | 23 | 0.722 | 1.789 | 8 | 0.581 | 2.343 |

properties.

The averaged values of the clustering coefficient over nodes C_{net} and the characteristic path length L_{net} were also obtained and the main observation is that,

as the threshold increases, the averaged clustering coefficient decreases and the characteristic path length increases. These changes were expected because the higher the threshold, more connections will be disregarded and as a result the nodes will become sparser. Because high clustering promotes functional overlap of densely connected neuronal elements and short paths promote effective interactions between these same elements (essential for functional integration), it's safe to say that by applying thresholds to the data there is a continuous loss of information regarding the effective integration of the brain regions.

Table 4.5: Scalar results that estimate the small-worldliness of a network.

| | γ | λ | σ |
|---------------|----------|-----------|----------|
| No Threshold | 1.075 | 0.981 | 1.096 |
| Threshold 0.2 | 1.508 | 1.051 | 1.435 |
| Threshold 0.4 | 2.966 | 1.312 | 2.261 |

The small-world network properties results are given in table 4.5, obtained using the following equations $\gamma = C_{net}/C_{rand} > 1$ and $\lambda = L_{net}/L_{rand} \simeq 1$. The scalar summary of small-worldliness can then be determined by the ratio $\sigma = \gamma/\lambda$, which should be > 1 . The small-world properties for these networks are evident for all thresholds, as indicated by $\sigma > 1$.

Figure 4.7 shows an anatomical map of the human brain functional network of one specific subject, for the three different thresholds. The spheres indicate the nodes and their sizes are proportional to the actual volume of the ROIs. As it was to be expected, as the value of the threshold increases, fewer connections survive and the graphs become subsequently sparser. It might not appear so, but when applying the 0.4 threshold some nodes became disconnected, in this situation path length is considered infinite, and thus the efficiency of the connection is zero.

Figure 4.8 shows how the degree of the nodes correlated with their cortical thickness. The values given by the t-test applied to this data are the following: for a no threshold scenario a $r = 0.118$ ($t = 0.968$; $p = 0.336$); for an applied threshold of 0.2 a $r = 0.007$ ($t = 0.053$; $p = 0.958$); and for a threshold of 0.4 a $r = 0.099$ ($t = 0.806$; $p = 0.423$). These results, and specially the small positive correlation observed for the three set-ups suggest that there is no significant association between these two properties.

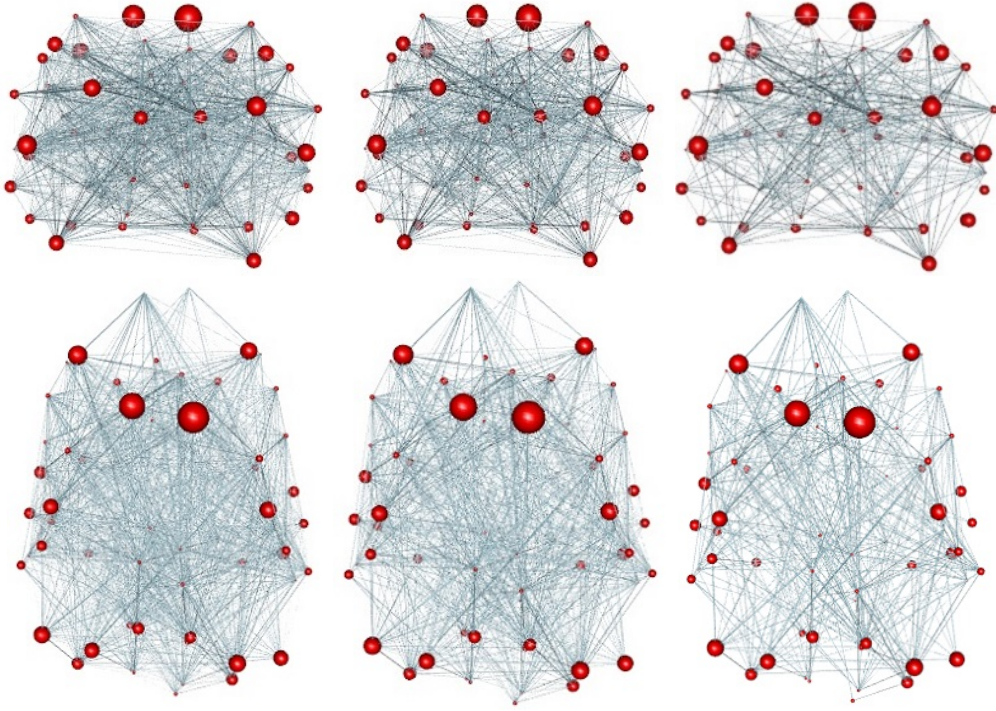


Figure 4.7: Correlation matrices visualized in anatomical space, for: (Left) No threshold; (Middle) Threshold at 0.2 and; (Right) Threshold at 0.4. The top images are presented in posterior coronal view, and the bottom ones in superior axial.

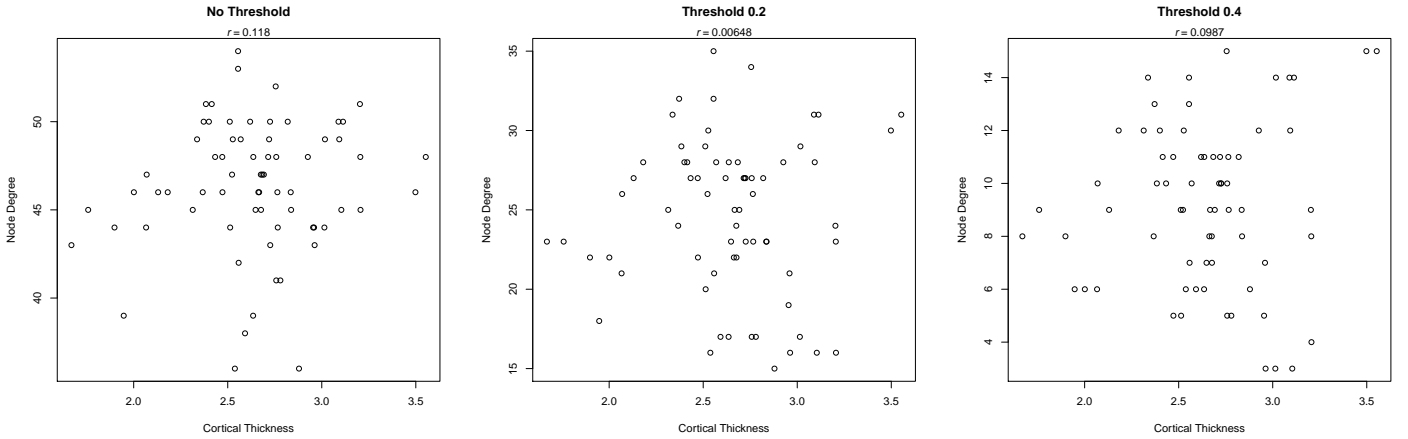


Figure 4.8: Degree K of each ROI against their cortical thickness, for the three different thresholds.

The same way, no significant correlation was found between cortical thickness and the clustering coefficient of each node, as can be seen in Figure 4.9 and by analyzing the results given by the t-test: for a no threshold scenario a $r = 0.019$ ($t = 0.153$; $p = 0.879$); for an applied threshold of 0.2 a $r = 0.195$ ($t = 1.614$; $p = 0.111$); and for a threshold of 0.4 a $r = -0.060$ ($t = -0.487$; $p = 0.628$).

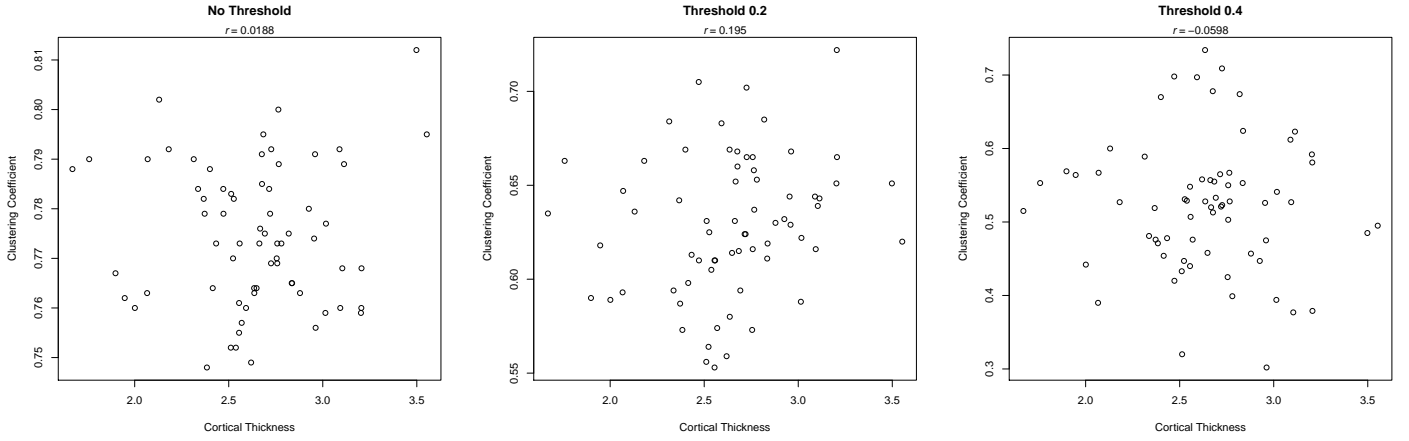


Figure 4.9: Clustering coefficient C of each ROI against their cortical thickness, for the three different thresholds.

As for the relation between cortical thickness and the mean minimum path length, figure 4.10, the results of the t-test are the following ones: for a no threshold scenario a $r = 0.119$ ($t = -0.974$; $p = 0.333$); for an applied threshold of 0.2 a $r = 0.027$ ($t = 0.216$; $p = 0.829$); and for a threshold of 0.4 a $r = -0.304$ ($t = -2.593$; $p = 0.012$). There is a strong negative correlation for the data to which was applied a threshold of 0.4, and because in this case t is lower than $t(66) = -1.997$ and p is below 5%, there is enough information to say that it is statistically significant. This means that the thicker the cortex region the shorter is the connection to any other region. This might mean that thicker regions may be connected to neighbouring regions, while thinner regions only connect to furthest regions.

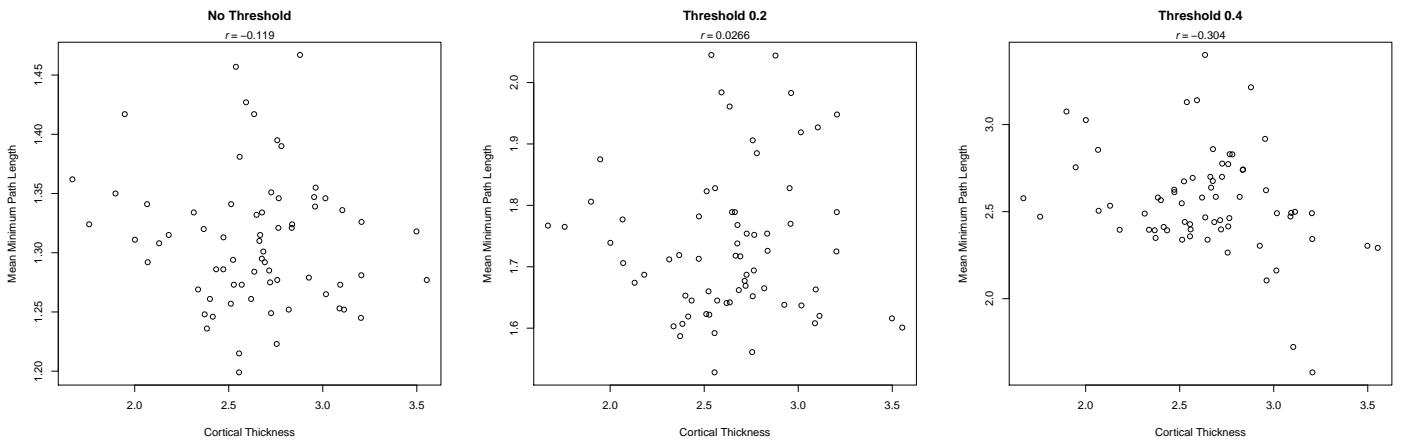


Figure 4.10: Mean minimum path length L of each ROI against their cortical thickness, for the three different thresholds.

4.5 Structural Analysis

Figure 4.11 represent the fiber tracks (for one subject) created by the diffusion toolbox and visualized with TrackVis, using the option to see only fibers with a minimum length of 12.5 mm.

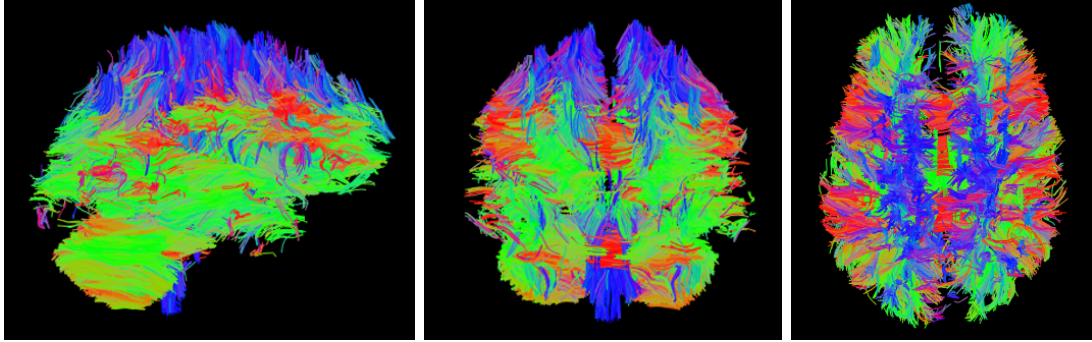


Figure 4.11: Visualization of the tracks file for subject one: (Left) sagittal; (Middle) anterior coronal and (Right) superior axial.

After obtaining all the fiber tracks for every subject and registering the parcellation file to the DTI space, it was possible to obtain the structural connectivity matrices. At this point the data consists in eighteen 68x68 undirected matrices, with the entries being the number of tracks between two particular ROIs. Figure 4.12 illustrate the connectivity matrix for one particular subject, as an example.

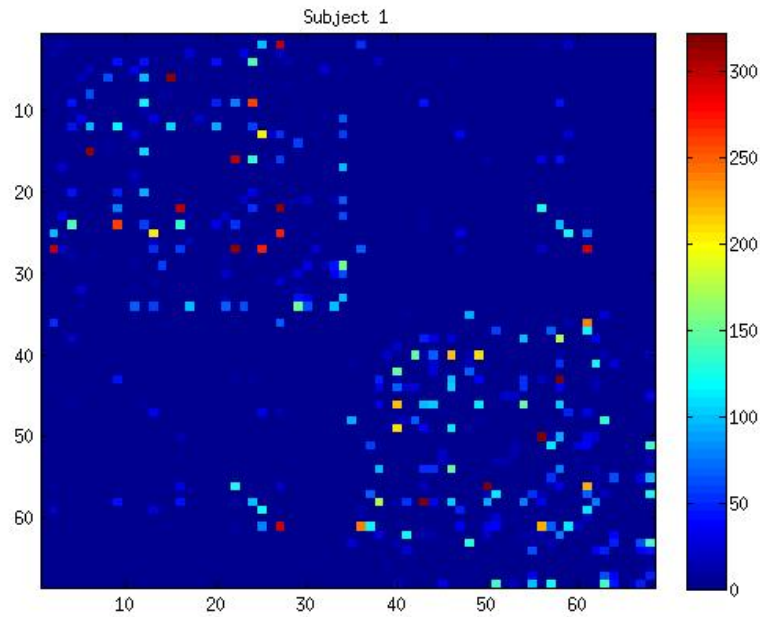


Figure 4.12: Structural connectivity matrix for subject one.

These matrices provide material for several types of analysis and studies. The structural analysis chosen for this project was a simpler one that consisted in summing all the entries for each ROI. The final result was a single matrix of 18x68 subjects and ROIs, respectively, with the entries representing the total number of tracks connected to one particular region.

This matrix was then normalized and the averages per subject and ROI were obtained. Figure 4.13 illustrates these values plotted against the averaged cortical thickness.

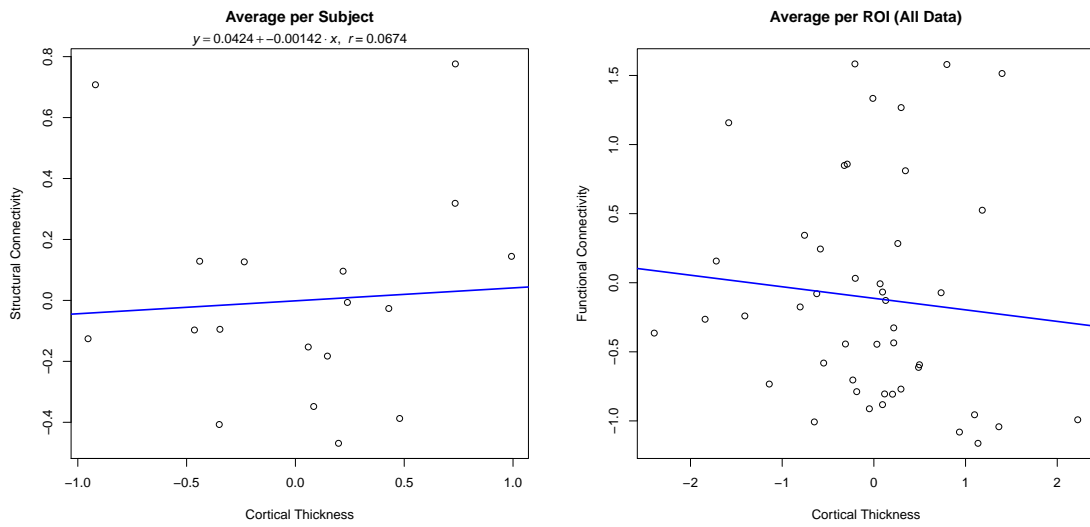


Figure 4.13: Average structural connectivity and cortical thickness per: (Left) subject; (Right) ROI.

The Pearson's' correlation coefficient was determined and tested by means of a t-test with 95% confidence interval, the null hypothesis being the non-existence of a relationship between number of fiber tracks and the cortical thickness. The results were the following: for the data averaged per subject a $r = 0.067$ ($t = 0.270$; $p = 0.790$); and the data averaged per ROI a $r = -0.096$ ($t = -0.631$; $p = 0.531$). With this information it is possible to conclude that there isn't any meaningful relation between cortical thickness of a region and its structural connectivity.

Chapter 5

Conclusion

The main goal of this project was to investigate how spontaneous neuronal activities in the human brain derived from resting-state BOLD signals relate with cortical thickness. Other brain connectivity measures were also used in order to complement the study, DTI data (number of tracks per region, in particular) and intrinsic properties of small-world networks (node degree, clustering coefficient and mean minimum path length) estimated using graph analysis on resting-state fMRI data.

Although the overall results suggest that there isn't any type of relation between cortical thickness and functional connectivity, structural connectivity and most of the properties of the brain small-world networks, there are some observations that should be retained:

- that the stronger pairwise functional connections were mostly symmetrically interhemispheric;
- thresholding the connectivity matrices doesn't lead to different results;
- The functional connectivity matrices and the measures of graph theory obtained from them, present small-world network properties, as it would be expected;
- the correlation between cortical thickness and the mean minimum path length was high enough to be statistically significant, suggesting that thicker regions might be connected to closer regions, while thinner regions might only connect to more distant regions;

- the fact that the functional connectivity and structural connectivity matrices are so different reflect not only direct, but also indirect anatomical connections.

There is still considerable skepticism regarding the correct interpretation of resting-state data and it is correct to assume resting-state approaches still have several methodological issues and need to go under technical optimization and experimental refinement in order to fully and correctly understand and interpret the results provided by the studies in this field.

The major strength of DTI is that it directly measures anatomic structure, but care must be taken when looking at complex fiber organization, such as crossing fibers. A suggestion of improvement for this project would be a more thorough preprocessing of the DTI data or even using other methods for diffusion tensor estimation and creation of fiber tracks.

Studying undirected binary matrices such as the ones used for the graph theory analysis in this project results in a significant loss of information. There is no possible way of knowing how strong a particular connection is, the same way that the possibility of knowing which areas are more influential and which are more influenced, by determining the indegree and outdegree, is lost as well. It would be interesting, in a further study, to take this information into account as well.

Another interesting study would be to investigate if the regions that are connected functionally or structurally, possess similar cortical thickness.

References

- ACHARD, S. AND BULLMORE, E. 2007. Efficiency and Cost of Economical Brain Functional Networks. *PLoS Comput. Biol.* 3, 2, e17.
- ACHARD, S., SALVADOR, R., WHITCHER, B., SUCKLING, J., AND BULLMORE, E. 2006. A Resilient, Low-Frequency, Small-World Human Brain Functional Network with Highly Connected Association Cortical Hubs. *J. Neurosci.* 26, 1, 63–72.
- ALBERT, R. AND BARABSI, A.-L. 2002. Statistical Mechanics of Complex Networks. *Rev. Mod. Phys* 74, 47–97.
- ALEXANDER-BLOCH, A., RAZNAHAN, A., BULLMORE, E., AND GIEDD, J. 2013. The Convergence of Maturational Change and Structural Covariance in Human Cortical Networks. *J. Neurosci.* 33, 7, 2889–2899.
- ANTICEVIC, A., COLE, M. W., MURRAY, J. D., CORLETT, P. R., WANG, X.-J., AND KRYSTAL, J. H. 2012. The role of default network deactivation in cognition and disease. *Trends in Cognitive Sciences* 16, 12, 584–592.
- ASHBURNER, J., BARNES, G., CHEN, C.-C., DAUNIZEAU, J., FLANDIN, G., FRISTON, K., GITELMAN, D., KIEBEL, S., KILNER, J., LITVAK, V., MORAN, R., PENNY, W., STEPHAN, K., GITELMAN, D., HENSON, R., HUTTON, C., GLAUCHE, V., MATTOU, J., AND PHILLIPS, C. 2012. *SPM8 Manual*. The FIL Methods Group.
- BASSETT, D. S. AND BULLMORE, E. 2006. Small-World Brain Networks. *Neuroscientist* 12, 6, 512–523.

- BECKMANN, C. F., DELUCA, M., DEVLIN, J. T., AND SMITH, S. M. 2005. Investigations into resting-state connectivity using independent component analysis. *Phil. Trans. R. Soc. B* 360, 1457, 1001–1013.
- BIHAN, D. L., MANGIN, J.-F., POUPON, C., CLARK, C. A., PAPPATA, S., MOLKO, N., AND CHABRIAT, H. 2001. Diffusion tensor imaging: Concepts and applications. *Journal of Magnetic Resonance Imaging* 13, 4, 534–546.
- BISWAL, B., YETKIN, F. Z., HAUGHTON, V. M., AND HYDE, J. S. 1995. Functional connectivity in the motor cortex of resting human brain using echo-planar MRI. *Magn. Reson. Med.* 34, 4, 537–541.
- BROSER, P. J., GROESCHEL, S., HAUSER, T.-K., LIDZBA, K., AND WILKE, M. 2012. Functional MRI-guided probabilistic tractography of cortico-cortical and cortico-subcortical language networks in children. *NeuroImage* 63, 3, 1561–1570.
- BULLMORE, E. AND SPORNS, O. 2009. Complex brain networks: graph theoretical analysis of structural and functional systems. *Nat. Rev. Neurosci.* 10, 3, 186–198.
- CHIALVO, D. R. 2004. Critical brain networks. *Physica A: Statistical Mechanics and its Applications* 340, 4, 756–765.
- CICCARELLI, O., CATANI, M., JOHANSEN-BERG, H., CLARK, C., AND THOMPSON, A. 2008. Diffusion-based tractography in neurological disorders: concepts, applications, and future developments. *The Lancet Neurology* 7, 8, 715–727.
- COHEN, A. L., FAIR, D. A., DOSENBACH, N. U. F., MIEZIN, F. M., DIERKER, D., ESSEN, D. C. V., SCHLAGGAR, B. L., AND PETERSEN, S. E. 2008. Defining Functional Areas in Individual Human Brains using Resting Functional Connectivity MRI. *Neuroimage* 41, 1, 45–57.
- COLE, D. M., SMITH, S. M., AND BECKMANN, C. F. 2010. Advances and pitfalls in the analysis and interpretation of resting-state FMRI data. *Front. Syst. Neurosci.* 4, 8, 1–8.

- CORDES, D., HAUGHTON, V. M., ARFANAKIS, K., WENDT, G. J., TURSKEI, P. A., MORITZ, C. H., QUIGLEY, M. A., AND MEYERAND, M. E. 2000. Mapping Functionally Related Regions of Brain with Functional Connectivity MR Imaging. *AJNR Am J Neuroradiol* 21, 9, 1636–1644.
- DALE, A. M., FISCHL, B., AND SERENO, M. I. 1999. Cortical Surface-Based Analysis: I. Segmentation and Surface Reconstruction. *NeuroImage* 9, 2, 179–194.
- DAMOISEAUX, J. S. 2009. Greater than the sum of its parts: a review of studies combining structural connectivity and resting-state functional connectivity. *Brain Struct Funct* 213, 6, 525–533.
- DECO, G. AND CORBETTA, M. 2011. The Dynamical Balance of the Brain at Rest. *Neuroscientist* 17, 1, 107–123.
- DIJK, K. V., HEDDEN, T., VENKATARAMAN, A., EVANS, K. C., LAZAR, S. W., AND BUCKNER, R. L. 2010. Intrinsic Functional Connectivity As a Tool For Human Connectomics: Theory, Properties, and Optimization. *J Neurophysiol* 103, 1, 297–321.
- DODEL, S., HERRMANN, J. M., AND GEISEL, T. 2002. Functional connectivity by cross-correlation clustering. *Neurocomputing* 44-46, 1064–1070.
- EGUILUZ, V. M., CHIALVO, D. R., CECCHI, G. A., BALIKI, M., AND APKARIAN, A. V. 2005. Scale-free brain functional networks. *Phys. Rev. Lett.* 94, 1, 018102.
- FAN, Y., SHI, F., SMITH, J. K., LIN, W., GILMORE, J. H., AND SHEN, D. 2011. Brain Anatomical Networks in Early Human Brain Development. *Neuroimage* 54, 3, 1862–1871.
- FARO, S. H., MOHAMED, F. B., LAW, M., AND ULMER, J. T. E. 2012. *Functional Neuroradiology: Principles and Clinical Applications*. Springer.
- FISCHL, B. AND DALE, A. M. 2000. Measuring the thickness of the human cerebral cortex from magnetic resonance images. *PNAS* 97, 20, 11050–11055.

- FISCHL, B., VAN DER KOUWE, A., DESTRIEUX, C., HALGREN, E., SGONNE, F., SALAT, D. H., BUSA, E., SEIDMAN, L. J., GOLDSTEIN, J., KENNEDY, D., CAVINESS, V., MAKRIS, N., ROSEN, B., AND DALE, A. M. 2004. Automatically parcellating the human cerebral cortex. *Cereb. Cortex* 14, 1, 11–22.
- FRISTON, K. J. 2003. *Human Brain Function*. Academic Press.
- FRISTON, K. J., FRITH, C. D., AND FRACKOWIAK, R. S. J. 1993. Time-dependent changes in effective connectivity measured with PET. *Human Brain Mapping* 1, 1, 69–79.
- GAZZANIGA, M., IVRY, R. B., AND MANGUN, G. R. 2008. *Cognitive Neuroscience: The Biology of the Mind*, Third Edition ed. W. W. Norton & Company.
- GONG, G., HE, Y., CONCHA, L., LEBEL, C., GROSS, D. W., EVANS, A. C., AND BEAULIEU, C. 2009. Mapping Anatomical Connectivity Patterns of Human Cerebral Cortex Using In Vivo Diffusion Tensor Imaging Tractography. *Cerebral Cortex* 19, 3, 524–536.
- GREICIUS, M. D., SUPEKAR, K., MENON, V., AND DOUGHERTY, R. F. 2009. Resting-State Functional Connectivity Reflects Structural Connectivity in the Default Mode Network. *Cereb. Cortex* 19, 1, 72–78.
- GUYE, M., BARTOLOMEI, F., AND RANJEVA, J.-P. 2008. Imaging structural and functional connectivity: towards a unified definition of human brain organization? *Curr. Opin. Neurol.* 21, 4, 393–403.
- HAGMANN, P., CAMMOUN, L., GIGANDET, X., MEULI, R., HONEY, C. J., WEDEEN, V. J., AND SPORNS, O. 2008. Mapping the Structural Core of Human Cerebral Cortex. *PLoS Biol* 6, 7, e159.
- HAMPSON, M., PETERSON, B. S., SKUDLARSKI, P., GATENBY, J. C., AND GORE, J. C. 2002. Detection of Functional Connectivity Using Temporal Correlations in MR Images. *Hum. Brain Mapp.* 15, 4, 247–262.

- HE, Y., CHEN, Z. J., AND EVANS, A. C. 2007. Small-World Anatomical Networks in the Human Brain Revealed by Cortical Thickness from MRI. *Cereb. Cortex* 17, 10, 2407–2419.
- HE, Y., WANG, J., WANG, L., CHEN, Z. J., YAN, C., YANG, H., TANG, H., ZHU, C., GONG, Q., ZANG, Y., AND EVANS, A. C. 2009. Uncovering Intrinsic Modular Organization of Spontaneous Brain Activity in Humans. *PLoS ONE* 4, 4, e5226.
- HOSSEINI, S. M. H. AND KESLER, S. R. 2013. Comparing connectivity pattern and small-world organization between structural correlation and resting-state networks in healthy adults. *NeuroImage* 78, 402–414.
- HOWELL, D. C. 2011. *Statistical Methods for Psychology, 8th ed.* Cengage Learning.
- HUETTEL, S. A., SONG, A. W., AND MCCARTHY, G. 2008. *Functional Magnetic Resonance Imaging.* Sinauer Associates.
- JENKINSON, M., BECKMANN, C. F., BEHRENS, T. E. J., WOOLRICH, M. W., AND SMITH, S. M. 2012. FSL. *NeuroImage* 62, 2, 782–790.
- JOHANSEN-BERG, H. AND BEHRENS, T. E. J. 2009. *Diffusion MRI: From Quantitative Measurement to In Vivo Neuroanatomy.* Academic Press.
- JONES, D. K. 2010. *Diffusion MRI: Theory, Methods, and Applications.* Oxford University Press, USA.
- KANDEL, E. R., SCHWARTZ, J. H., AND JESSELL, T. M. 2000. *Principles of Neural Science*, 4th Edition ed. McGraw-Hill.
- KOCH, M. A., NORRIS, D. G., AND HUND-GEORGIADIS, M. 2002. An Investigation of Functional and Anatomical Connectivity Using Magnetic Resonance Imaging. *NeuroImage* 16, 1, 241–250.
- KOYAMA, M. S., KELLY, C., SHEHZAD, Z., PENESETTI, D., CASTELLANOS, F. X., AND MILHAM, M. P. 2010. Reading Networks at Rest. *Cereb. Cortex* 20, 11, 2549–2559.

- LEE, M. H., SMYSER, C. D., AND SHIMONY, J. S. 2012. Resting-State fMRI: A Review of Methods and Clinical Applications. *AJNR Am J Neuroradiol* 34, 1866–1872.
- LI, K., GUO, L., NIE, J., LI, G., AND LIU, T. 2009. Review of methods for functional brain connectivity detection using fMRI. *Comput Med Imaging Graph* 33, 2, 131–139.
- MARGULIES, D. S., BTTGER, J., LONG, X., LV, Y., KELLY, C., SCHFER, A., GOLDHAHN, D., ABBUSHI, A., MILHAM, M. P., LOHMANN, G., AND VILLRINGER, A. 2010. Resting developments: a review of fMRI post-processing methodologies for spontaneous brain activity. *Magn Reson Mater Phy* 23, 5-6, 289–307.
- MCRROBBIE, D. W. 2007. *MRI from Picture to Proton*. Cambridge University Press.
- MORI, S., CRAIN, B. J., CHACKO, V. P., AND ZIJL, P. C. M. V. 1999. Three-dimensional tracking of axonal projections in the brain by magnetic resonance imaging. *Annals of Neurology* 45, 2, 265–269.
- REIJNEVELD, J. C., PONTEN, S. C., BERENDSE, H. W., AND STAM, C. J. 2007. The application of graph theoretical analysis to complex networks in the brain. *Clin Neurophysiol* 118, 11, 2317–2331.
- RIBEIRO, A. S., LACERDA, L., RODRIGUES, J., SOUSA, J. M., AND FERREIRA, H. A. 2013. Multimodal Imaging Brain Connectivity Analysis. Vol. epos 296.
- ROGERS, B. P., MORGAN, V. L., NEWTON, A. T., AND GORE, J. C. 2007. Assessing Functional Connectivity in the Human Brain by FMRI. *Magn. Reson. Imaging* 25, 10, 1347–1357.
- RUBINOV, M. AND SPORNS, O. 2010. Complex network measures of brain connectivity: Uses and interpretations. *NeuroImage* 52, 3, 1059–1069.
- SALVADOR, R., SUCKLING, J., COLEMAN, M. R., PICKARD, J. D., MENON, D., AND BULLMORE, E. 2005. Neurophysiological Architecture of Functional Magnetic Resonance Images of Human Brain. *Cereb. Cortex* 15, 9, 1332–1342.

- SALVADOR, R., SUCKLING, J., SCHWARZBAUER, C., AND BULLMORE, E. 2005. Undirected graphs of frequency-dependent functional connectivity in whole brain networks. *Philos Trans R Soc Lond B Biol Sci* 360, 1457, 937–946.
- SANZ-ARIGITA, E. J., SCHOONHEIM, M. M., DAMOISEAUX, J. S., ROMBOUTS, S. A. R. B., MARIS, E., BARKHOF, F., SCHELTENS, P., AND STAM, C. J. 2010. Loss of "Small-World" Networks in Alzheimer's Disease: Graph Analysis of fMRI Resting-State Functional Connectivity. *PLoS ONE* 5, 11, e13788.
- SCHMAHMANN, J. D. AND PANDYA, D. 2009. *Fiber Pathways of the Brain*. Oxford University Press, USA.
- SEGALL, J. M., ALLEN, E. A., JUNG, R. E., ERHARDT, E. B., ARJA, S. K., KIEHL, K., AND CALHOUN, V. D. 2012. Correspondence between structure and function in the human brain at rest. *Front Neuroinform* 6, 10.
- SMITH, S. M. 2002. Fast robust automated brain extraction. *Hum Brain Mapp* 17, 3, 143–155.
- SPORNS, O. 2011. *Networks of the Brain*. MIT Press.
- SPORNS, O. AND ZWI, J. D. 2004. The Small World of the Cerebral Cortex. *Neuroinform* 2, 2, 145–162.
- STAM, C. J. AND REIJNEVELD, J. C. 2007. Graph theoretical analysis of complex networks in the brain. *Nonlinear Biomed Phys* 1, 1, 1–3.
- VAN DEN HEUVEL, M. P. AND POL, H. E. H. 2010. Exploring the brain network: A review on resting-state fMRI functional connectivity. *European Neuropsychopharmacology* 20, 8, 519–534.
- WANG, R., BENNER, T., SORENSSEN, A. G., AND WEDEEN, V. J. 2007. Diffusion Toolkit: A Software Package for Diffusion Imaging Data Processing and Tractography. *Proc. Intl. Soc. Mag. Reson. Med.* 15.
- WANG, R. AND WEDEEN, V. J. 2006-2010. TrackVis.org.

- WHITFIELD-GABRIELI, S. AND NIETO-CASTANON, A. 2012. Conn: a functional connectivity toolbox for correlated and anticorrelated brain networks. *Brain connectivity* 2, 3, 123–141.

Appendices

Appendix A

Cortical thickness

Table A.1: Cortical thickness (mm) of 68 ROIs (left and right hemispheres) for subjects one to eleven.

| ROI | Subject 1 | | Subject 2 | | Subject 3 | | Subject 4 | | Subject 5 | | Subject 6 | | Subject 7 | | Subject 8 | | Subject 9 | | Subject 10 | | Subject 11 | |
|----------------------------|-----------|-----|-----------|-----|-----------|-----|-----------|-----|-----------|-----|-----------|-----|-----------|-----|-----------|-----|-----------|-----|------------|-----|------------|-----|
| | LH | RH | LH | RH | LH | RH | LH | RH | LH | RH | LH | RH | LH | RH | LH | RH | LH | RH | LH | RH | LH | RH |
| Bankssts | 1.9 | 2.7 | 2.6 | 2.9 | 1.9 | 2.7 | 2.7 | 2.7 | 2.9 | 2.8 | 2.2 | 2.4 | 1.9 | 2.8 | 1.8 | 2.4 | 2.4 | 2.8 | 2.4 | 2.7 | 2.6 | 2.8 |
| | 2.4 | 2.4 | 2.9 | 2.6 | 2.6 | 2.4 | 2.4 | 2.8 | 2.9 | 2.9 | 2.3 | 2.4 | 2.5 | 2.7 | 2.6 | 2.6 | 2.6 | 2.5 | 2.5 | 2.8 | 2.9 | 2.6 |
| Caudal Anterior Cingulate | 2.7 | 2.9 | 2.7 | 2.7 | 2.8 | 2.9 | 2.9 | 2.8 | 2.9 | 3.0 | 2.6 | 2.5 | 2.8 | 2.8 | 2.6 | 2.6 | 2.7 | 2.6 | 2.5 | 2.6 | 2.7 | |
| Caudal Middle Frontal | | | | | | | | | | | | | | | | | | | | | | |
| Cuneus | 1.9 | 2.0 | 1.9 | 1.8 | 2.0 | 1.9 | 2.1 | 2.1 | 2.3 | 2.1 | 1.9 | 2.0 | 1.9 | 1.9 | 1.9 | 1.9 | 1.6 | 1.8 | 1.9 | 2.0 | 2.0 | |
| Entorhinal | 2.9 | 3.1 | 3.2 | 3.4 | 3.4 | 3.0 | 3.7 | 4.1 | 3.4 | 3.5 | 3.04 | 3.5 | 3.1 | 2.9 | 3.1 | 3.5 | 3.6 | 3.5 | 2.2 | 2.9 | 3.1 | 2.9 |
| Fusiform | 3.0 | 2.8 | 2.9 | 3.0 | 2.8 | 2.8 | 2.7 | 2.8 | 2.8 | 3.0 | 2.6 | 2.7 | 2.8 | 2.7 | 2.8 | 2.7 | 2.6 | 2.8 | 2.8 | 2.7 | 2.6 | |
| Inferior Parietal | 2.7 | 2.7 | 2.6 | 2.7 | 2.6 | 2.7 | 2.6 | 2.8 | 2.6 | 2.4 | 2.5 | 2.6 | 2.7 | 2.3 | 2.4 | 2.5 | 2.6 | 2.4 | 2.6 | 2.7 | 2.6 | |
| Inferior Temporal | 2.5 | 2.9 | 2.7 | 3.0 | 2.8 | 3.0 | 2.7 | 3.1 | 2.6 | 2.8 | 2.5 | 2.9 | 2.9 | 3.2 | 2.6 | 2.6 | 2.8 | 2.9 | 2.7 | 2.9 | 2.7 | 2.8 |
| Isthmus Cingulate | 2.5 | 2.3 | 2.6 | 2.3 | 2.5 | 2.5 | 2.6 | 2.6 | 2.4 | 2.6 | 2.3 | 2.3 | 2.5 | 2.7 | 2.5 | 2.5 | 2.6 | 2.5 | 2.6 | 2.4 | 2.6 | |
| Lateral Occipital | 2.2 | 2.4 | 2.3 | 2.3 | 2.2 | 2.3 | 2.3 | 2.5 | 2.3 | 2.4 | 2.1 | 2.2 | 2.3 | 2.3 | 2.2 | 2.2 | 2.2 | 2.3 | 2.1 | 2.3 | 2.1 | 2.3 |
| Lateral Orbito Frontal | 2.9 | 2.9 | 2.8 | 2.9 | 2.8 | 2.9 | 3.0 | 3.1 | 3.1 | 2.6 | 2.7 | 2.8 | 2.9 | 2.7 | 2.8 | 2.9 | 2.0 | 1.8 | 2.0 | 2.0 | 1.9 | 2.0 |
| Lingual | 2.1 | 2.2 | 2.0 | 2.1 | 2.2 | 2.2 | 2.2 | 2.2 | 2.2 | 2.3 | 1.9 | 2.0 | 1.8 | 1.9 | 2.0 | 1.8 | 2.0 | 2.0 | 2.0 | 1.9 | 2.0 | |
| Medial Orbito Frontal | 2.9 | 2.6 | 2.6 | 2.7 | 2.6 | 2.6 | 2.7 | 2.7 | 2.8 | 2.8 | 2.5 | 2.6 | 2.8 | 2.6 | 2.6 | 2.6 | 2.7 | 2.7 | 2.6 | 2.8 | 2.6 | 2.6 |
| Middle Temporal | 2.2 | 2.8 | 2.6 | 3.0 | 2.6 | 3.1 | 2.6 | 2.9 | 2.6 | 2.9 | 2.4 | 2.7 | 2.6 | 3.0 | 2.2 | 2.7 | 2.4 | 2.6 | 2.4 | 2.9 | 2.9 | 3.1 |
| Parahippocampal | 3.0 | 2.8 | 3.0 | 2.8 | 2.8 | 2.5 | 2.7 | 2.7 | 3.3 | 3.3 | 2.2 | 2.3 | 2.8 | 2.6 | 2.8 | 2.9 | 2.9 | 2.9 | 2.6 | 2.8 | 2.3 | 2.3 |
| Paracentral | 2.5 | 2.6 | 2.4 | 2.4 | 2.3 | 2.4 | 2.3 | 2.4 | 2.6 | 2.5 | 2.2 | 2.3 | 2.4 | 2.3 | 2.1 | 2.1 | 2.4 | 2.3 | 2.2 | 2.2 | 2.2 | 2.2 |
| Parsopercularis | 2.9 | 2.8 | 2.5 | 2.8 | 2.7 | 2.9 | 2.8 | 2.8 | 2.8 | 2.8 | 2.6 | 2.7 | 2.6 | 2.8 | 2.5 | 2.7 | 2.9 | 3.0 | 2.7 | 2.8 | 2.6 | 2.6 |
| Parsorbitalis | 3.0 | 2.8 | 3.0 | 3.0 | 3.2 | 3.1 | 3.2 | 3.2 | 3.2 | 3.1 | 2.8 | 2.7 | 3.1 | 2.8 | 2.6 | 2.6 | 2.8 | 2.7 | 2.9 | 3.0 | 2.8 | 3.0 |
| Parstriangularis | 2.9 | 2.7 | 2.6 | 2.8 | 2.8 | 2.7 | 2.9 | 2.9 | 2.9 | 3.0 | 2.5 | 2.8 | 2.5 | 2.9 | 2.4 | 2.6 | 2.7 | 2.7 | 2.7 | 2.8 | 2.6 | 2.6 |
| Pericalcarine | 1.8 | 1.7 | 1.6 | 1.7 | 2.1 | 2.1 | 1.8 | 1.8 | 1.8 | 2.1 | 1.8 | 1.8 | 1.4 | 1.6 | 1.7 | 1.8 | 1.7 | 1.8 | 1.7 | 1.8 | 1.7 | 1.7 |
| Postcentral | 2.0 | 2.2 | 2.3 | 2.3 | 2.2 | 2.2 | 2.1 | 2.2 | 2.2 | 2.3 | 2.0 | 2.1 | 2.1 | 2.1 | 1.7 | 1.9 | 1.9 | 2.0 | 2.0 | 1.8 | 2.0 | |
| Posterior cingulate | 2.7 | 2.5 | 2.5 | 2.5 | 2.5 | 2.6 | 2.6 | 2.4 | 2.7 | 2.7 | 2.3 | 2.4 | 2.6 | 2.7 | 2.5 | 2.5 | 2.7 | 2.5 | 2.5 | 2.6 | 2.8 | 2.5 |
| Precentral | 2.4 | 2.5 | 2.4 | 2.5 | 2.6 | 2.6 | 2.5 | 2.5 | 2.7 | 2.7 | 2.3 | 2.3 | 2.5 | 2.7 | 1.9 | 2.1 | 2.4 | 2.6 | 2.2 | 2.3 | 2.1 | 2.3 |
| Precuneus | 2.6 | 2.5 | 2.6 | 2.6 | 2.6 | 2.6 | 2.7 | 2.6 | 2.8 | 2.6 | 2.4 | 2.5 | 2.7 | 2.5 | 2.6 | 2.4 | 2.4 | 2.4 | 2.4 | 2.5 | 2.6 | 2.4 |
| Rostral Anterior Cingulate | 3.0 | 3.0 | 3.1 | 3.0 | 2.6 | 2.7 | 2.9 | 3.2 | 3.5 | 3.3 | 2.9 | 2.8 | 3.0 | 3.2 | 3.1 | 3.2 | 2.9 | 3.0 | 3.3 | 2.8 | 3.2 | 2.9 |
| Rostral Middle Frontal | 2.7 | 2.7 | 2.6 | 2.7 | 2.7 | 2.7 | 2.7 | 2.7 | 2.8 | 2.8 | 2.5 | 2.6 | 2.6 | 2.7 | 2.4 | 2.4 | 2.5 | 2.6 | 2.6 | 2.7 | 2.5 | 2.5 |
| Superior Frontal | 3.0 | 2.9 | 2.9 | 3.0 | 3.1 | 3.1 | 2.9 | 3.0 | 3.1 | 3.1 | 2.8 | 2.8 | 3.0 | 3.0 | 2.8 | 2.8 | 2.9 | 2.9 | 2.8 | 2.9 | 3.0 | 2.9 |
| Superior Parietal | 2.5 | 2.6 | 2.4 | 2.5 | 2.5 | 2.5 | 2.5 | 2.5 | 2.6 | 2.5 | 2.4 | 2.4 | 2.4 | 2.4 | 2.3 | 2.3 | 2.3 | 2.4 | 2.3 | 2.3 | 2.4 | 2.4 |
| Superior Temporal | 2.6 | 2.9 | 2.6 | 2.8 | 2.5 | 2.8 | 2.7 | 2.8 | 2.8 | 2.8 | 2.3 | 2.7 | 2.5 | 2.8 | 2.4 | 2.6 | 2.5 | 2.6 | 2.5 | 2.6 | 2.6 | 2.9 |
| Supramarginal | 2.2 | 2.7 | 2.3 | 2.7 | 2.2 | 2.8 | 2.5 | 2.5 | 2.5 | 2.6 | 2.2 | 2.5 | 2.5 | 2.5 | 2.0 | 2.3 | 2.2 | 2.6 | 2.3 | 2.5 | 2.4 | 2.6 |
| Frontal Pole | 2.9 | 2.9 | 3.1 | 2.8 | 3.2 | 3.1 | 2.8 | 3.3 | 3.2 | 3.4 | 2.9 | 2.8 | 3.3 | 3.2 | 3.2 | 3.0 | 3.0 | 3.0 | 2.8 | 2.8 | 3.0 | 3.1 |
| Temporal Pole | 4.2 | 4.2 | 3.9 | 4.0 | 3.7 | 4.3 | 3.8 | 3.2 | 3.3 | 3.6 | 3.6 | 2.9 | 3.9 | 3.6 | 3.5 | 4.0 | 3.7 | 3.6 | 3.6 | 3.7 | 3.5 | 3.3 |
| Transverse Temporal | 2.6 | 2.5 | 2.5 | 2.4 | 2.7 | 2.7 | 2.6 | 2.6 | 2.9 | 2.7 | 2.0 | 2.4 | 2.5 | 2.6 | 2.5 | 2.2 | 2.6 | 2.4 | 2.5 | 2.1 | 2.4 | 2.5 |
| Insula | 3.3 | 3.5 | 3.0 | 3.3 | 3.0 | 3.2 | 3.3 | 3.2 | 3.4 | 3.5 | 3.0 | 2.9 | 3.2 | 3.2 | 3.2 | 3.1 | 3.2 | 3.3 | 3.2 | 3.3 | 3.0 | 3.2 |

Table A.2: Cortical thickness (mm) of 68 ROIs (left and right hemispheres) for subjects twelve to twenty-two

| ROI | Subject 12 | | Subject 13 | | Subject 14 | | Subject 15 | | Subject 16 | | Subject 17 | | Subject 18 | | Subject 19 | | Subject 20 | | Subject 21 | | Subject 22 | |
|----------------------------|------------|-----|------------|------|------------|-----|------------|-----|------------|-----|------------|-----|------------|-----|------------|-----|------------|-----|------------|-----|------------|-----|
| | LH | RH | LH | RH | LH | RH | LH | RH | LH | RH | LH | RH | LH | RH | LH | RH | LH | RH | LH | RH | LH | RH |
| Bankssts | 2.7 | 2.5 | 2.3 | 2.6 | 2.7 | 2.7 | 2.5 | 2.7 | 2.4 | 2.5 | 2.8 | 2.8 | 1.5 | 2.6 | 2.8 | 2.9 | 2.6 | 2.9 | 2.4 | 2.4 | 2.4 | 2.8 |
| Caudal Anterior Cingulate | 2.7 | 2.9 | 2.5 | 2.5 | 3.1 | 2.6 | 3.1 | 3.1 | 2.5 | 2.6 | 3.2 | 3.1 | 2.4 | 2.3 | 2.8 | 2.8 | 2.6 | 2.7 | 3.1 | 2.8 | 2.4 | 2.7 |
| Caudal Middle Frontal | 2.9 | 2.8 | 2.9 | 2.9 | 2.7 | 2.8 | 2.8 | 2.8 | 2.7 | 2.6 | 2.9 | 3.0 | 2.5 | 2.6 | 2.8 | 2.6 | 2.9 | 2.9 | 2.6 | 2.7 | 2.6 | 2.8 |
| Cuneus | 2.0 | 2.2 | 1.7 | 2.0 | 1.8 | 1.8 | 1.9 | 1.7 | 2.0 | 2.0 | 1.9 | 2.2 | 1.6 | 2.0 | 1.8 | 1.8 | 2.0 | 2.0 | 1.9 | 2.2 | 1.8 | 1.8 |
| Entorhinal | 2.4 | 2.6 | 3.4 | 3.3 | 2.3 | 2.4 | 2.7 | 3.8 | 3.5 | 3.4 | 3.4 | 3.0 | 2.8 | 3.1 | 2.5 | 2.5 | 3.1 | 3.2 | 3.9 | 3.7 | 3.4 | 3.3 |
| Fusiform | 2.7 | 2.8 | 2.9 | 2.7 | 2.8 | 2.8 | 2.7 | 2.7 | 2.8 | 2.7 | 2.8 | 2.7 | 2.6 | 2.6 | 2.8 | 2.8 | 2.9 | 2.8 | 2.9 | 2.9 | 2.9 | 2.8 |
| Inferior Parietal | 2.9 | 2.8 | 2.6 | 2.5 | 2.5 | 2.6 | 2.3 | 2.8 | 2.7 | 2.5 | 2.7 | 2.9 | 2.1 | 2.6 | 2.7 | 2.8 | 2.7 | 2.8 | 2.5 | 2.6 | 2.6 | 2.5 |
| Inferior Temporal | 3.1 | 3.1 | 2.8 | 3.1 | 2.7 | 3.0 | 2.7 | 3.0 | 2.9 | 2.7 | 2.8 | 3.0 | 2.6 | 2.8 | 2.7 | 3.1 | 2.8 | 3.0 | 2.6 | 2.6 | 2.7 | 2.9 |
| Isthmus Cingulate | 2.6 | 2.7 | 2.7 | 2.7 | 2.4 | 2.5 | 2.8 | 2.8 | 2.4 | 2.2 | 2.5 | 2.5 | 2.6 | 2.4 | 2.5 | 2.4 | 2.7 | 2.5 | 2.6 | 2.8 | 2.4 | 2.5 |
| Lateral Occipital | 2.3 | 2.5 | 2.1 | 2.3 | 2.1 | 2.3 | 2.0 | 2.2 | 2.2 | 2.3 | 2.2 | 2.4 | 2.0 | 2.1 | 2.0 | 2.2 | 2.4 | 2.5 | 2.3 | 2.5 | 2.2 | 2.2 |
| Lateral Orbito Frontal | 2.9 | 3.0 | 3.1 | 3.0 | 3.0 | 3.0 | 2.8 | 2.9 | 2.6 | 2.9 | 2.8 | 2.3 | 2.6 | 3.0 | 3.0 | 2.9 | 2.9 | 2.6 | 2.9 | 2.9 | 3.0 | 2.8 |
| Lingual | 2.2 | 2.2 | 2.0 | 2.0 | 2.0 | 2.0 | 1.9 | 2.0 | 2.0 | 2.1 | 1.9 | 2.1 | 1.7 | 1.8 | 2.0 | 2.1 | 2.1 | 2.1 | 2.2 | 2.2 | 1.8 | 2.0 |
| Medial Orbito Frontal | 2.9 | 2.7 | 3.0 | 2.8 | 2.7 | 2.6 | 2.8 | 2.6 | 2.7 | 2.5 | 2.8 | 2.8 | 2.3 | 2.3 | 2.8 | 2.7 | 2.5 | 2.9 | 2.8 | 2.9 | 2.6 | 2.8 |
| Middle Temporal | 2.9 | 3.0 | 2.6 | 2.9 | 2.5 | 2.9 | 2.5 | 3.1 | 2.5 | 2.5 | 2.8 | 3.0 | 2.4 | 2.8 | 2.6 | 3.0 | 2.7 | 3.1 | 2.5 | 2.7 | 2.5 | 2.8 |
| Parahippocampal | 2.4 | 2.4 | 2.9 | 2.6 | 2.2 | 2.7 | 3.2 | 2.8 | 2.6 | 3.1 | 2.9 | 2.7 | 2.6 | 2.2 | 2.4 | 2.6 | 2.8 | 2.8 | 3.1 | 3.1 | 3.3 | 3.1 |
| Paracentral | 2.3 | 2.4 | 2.4 | 2.4 | 2.3 | 2.4 | 2.3 | 2.4 | 2.4 | 2.3 | 2.6 | 2.6 | 2.2 | 2.3 | 2.3 | 2.6 | 2.5 | 2.4 | 2.4 | 2.4 | 2.2 | 2.4 |
| Parsopercularis | 2.9 | 3.0 | 2.8 | 2.8 | 2.5 | 2.9 | 2.8 | 2.9 | 2.6 | 2.7 | 2.8 | 2.9 | 2.4 | 2.6 | 2.9 | 2.9 | 2.9 | 3.0 | 2.8 | 2.8 | 2.8 | 2.8 |
| Parsorbitalis | 2.9 | 3.3 | 3.2 | 2.9 | 2.9 | 2.8 | 3.2 | 3.0 | 2.9 | 2.7 | 3.3 | 3.4 | 3.0 | 2.9 | 3.2 | 3.0 | 3.1 | 2.8 | 2.9 | 3.1 | 3.2 | 3.0 |
| Parsstriangularis | 2.8 | 2.9 | 2.8 | 2.7 | 2.7 | 2.7 | 2.7 | 2.8 | 2.7 | 2.8 | 2.7 | 3.0 | 2.5 | 2.7 | 2.7 | 2.7 | 2.8 | 2.6 | 2.7 | 2.9 | 2.5 | 2.8 |
| Pericalcarine | 2.0 | 2.0 | 1.7 | 1.7 | 1.8 | 1.7 | 1.5 | 1.6 | 1.5 | 1.7 | 1.6 | 1.7 | 1.5 | 1.8 | 1.6 | 1.8 | 1.7 | 1.7 | 1.6 | 1.8 | 1.3 | 1.3 |
| Postcentral | 2.3 | 2.3 | 2.3 | 2.3 | 1.9 | 2.1 | 2.1 | 2.0 | 2.1 | 2.0 | 2.1 | 2.2 | 2.0 | 2.2 | 2.2 | 2.4 | 2.3 | 2.2 | 2.2 | 1.9 | 1.9 | 2.0 |
| Posterior cingulate | 2.7 | 2.8 | 2.7 | 2.7 | 2.8 | 2.6 | 2.7 | 2.7 | 2.6 | 2.6 | 2.8 | 2.7 | 2.5 | 2.5 | 2.7 | 2.7 | 2.7 | 2.5 | 2.9 | 2.8 | 2.6 | 2.5 |
| Precentral | 2.7 | 2.6 | 2.6 | 2.7 | 2.2 | 2.4 | 2.4 | 2.5 | 2.3 | 2.4 | 2.5 | 2.6 | 2.4 | 2.4 | 2.6 | 2.7 | 2.5 | 2.4 | 2.5 | 2.4 | 2.2 | 2.2 |
| Precuneus | 2.7 | 2.6 | 2.5 | 2.5 | 2.5 | 2.5 | 2.6 | 2.6 | 2.5 | 2.5 | 2.7 | 2.7 | 2.3 | 2.3 | 2.6 | 2.5 | 2.7 | 2.6 | 2.6 | 2.8 | 2.3 | 2.4 |
| Rostral Anterior Cingulate | 3.2 | 3.2 | 3.2 | 3.2 | 3.2 | 3.2 | 3.2 | 3.1 | 3.1 | 3.4 | 3.3 | 3.4 | 2.8 | 2.8 | 3.4 | 3.0 | 3.2 | 3.2 | 3.4 | 3.2 | 3.2 | 3.3 |
| Rostral Middle Frontal | 2.7 | 2.7 | 2.8 | 2.8 | 2.6 | 2.6 | 2.6 | 2.6 | 2.4 | 2.8 | 2.8 | 2.4 | 2.5 | 2.7 | 2.7 | 2.7 | 2.6 | 2.7 | 2.8 | 2.7 | 2.6 | 2.6 |
| Superior Frontal | 3.0 | 3.1 | 3.1 | 3.0 | 3.0 | 3.0 | 3.0 | 3.0 | 2.9 | 2.9 | 3.1 | 3.2 | 2.7 | 2.7 | 3.0 | 3.0 | 3.0 | 3.0 | 3.1 | 3.1 | 3.0 | 2.9 |
| Superior Parietal | 2.5 | 2.6 | 2.4 | 2.4 | 2.4 | 2.4 | 2.3 | 2.4 | 2.5 | 2.5 | 2.5 | 2.6 | 2.3 | 2.3 | 2.4 | 2.5 | 2.6 | 2.5 | 2.4 | 2.3 | 2.3 | 2.3 |
| Superior Temporal | 2.9 | 2.9 | 2.6 | 2.9 | 2.5 | 2.8 | 2.6 | 2.8 | 2.5 | 2.7 | 2.5 | 2.8 | 2.1 | 2.5 | 2.7 | 2.7 | 2.7 | 3.0 | 2.7 | 2.8 | 2.5 | 2.6 |
| Supramarginal | 2.7 | 2.6 | 2.5 | 2.6 | 2.4 | 2.4 | 2.3 | 2.8 | 2.4 | 2.4 | 2.5 | 2.7 | 2.3 | 2.4 | 2.6 | 2.8 | 2.6 | 2.7 | 2.5 | 2.6 | 2.4 | 2.3 |
| Frontal Pole | 3.2 | 3.0 | 3.2 | 3.1 | 2.9 | 2.8 | 3.4 | 3.4 | 3.2 | 2.7 | 3.2 | 3.5 | 3.0 | 2.6 | 3.3 | 2.9 | 3.1 | 3.1 | 3.2 | 2.9 | 2.8 | 3.0 |
| Temporal Pole | 2.9 | 2.4 | 3.8 | 3.3 | 2.8 | 3.2 | 3.1 | 3.4 | 4.1 | 3.0 | 3.6 | 3.5 | 3.2 | 3.1 | 3.0 | 2.8 | 3.6 | 3.6 | 4.0 | 4.6 | 3.7 | 3.9 |
| Transverse Temporal | 3.0 | 2.7 | 2.6 | 3.0 | 2.4 | 2.4 | 2.5 | 2.4 | 2.3 | 2.9 | 2.7 | 2.3 | 1.8 | 2.1 | 2.7 | 2.6 | 2.5 | 2.5 | 2.6 | 2.2 | 2.5 | 2.4 |
| Insula | 3.4 | 3.5 | 3.4 | 3.26 | 3.2 | 3.3 | 3.3 | 3.2 | 3.2 | 2.6 | 3.2 | 3.4 | 3.0 | 3.2 | 3.2 | 3.0 | 3.1 | 3.2 | 3.5 | 3.4 | 3.4 | 3.1 |

Appendix B

Correlation Coefficient Maps

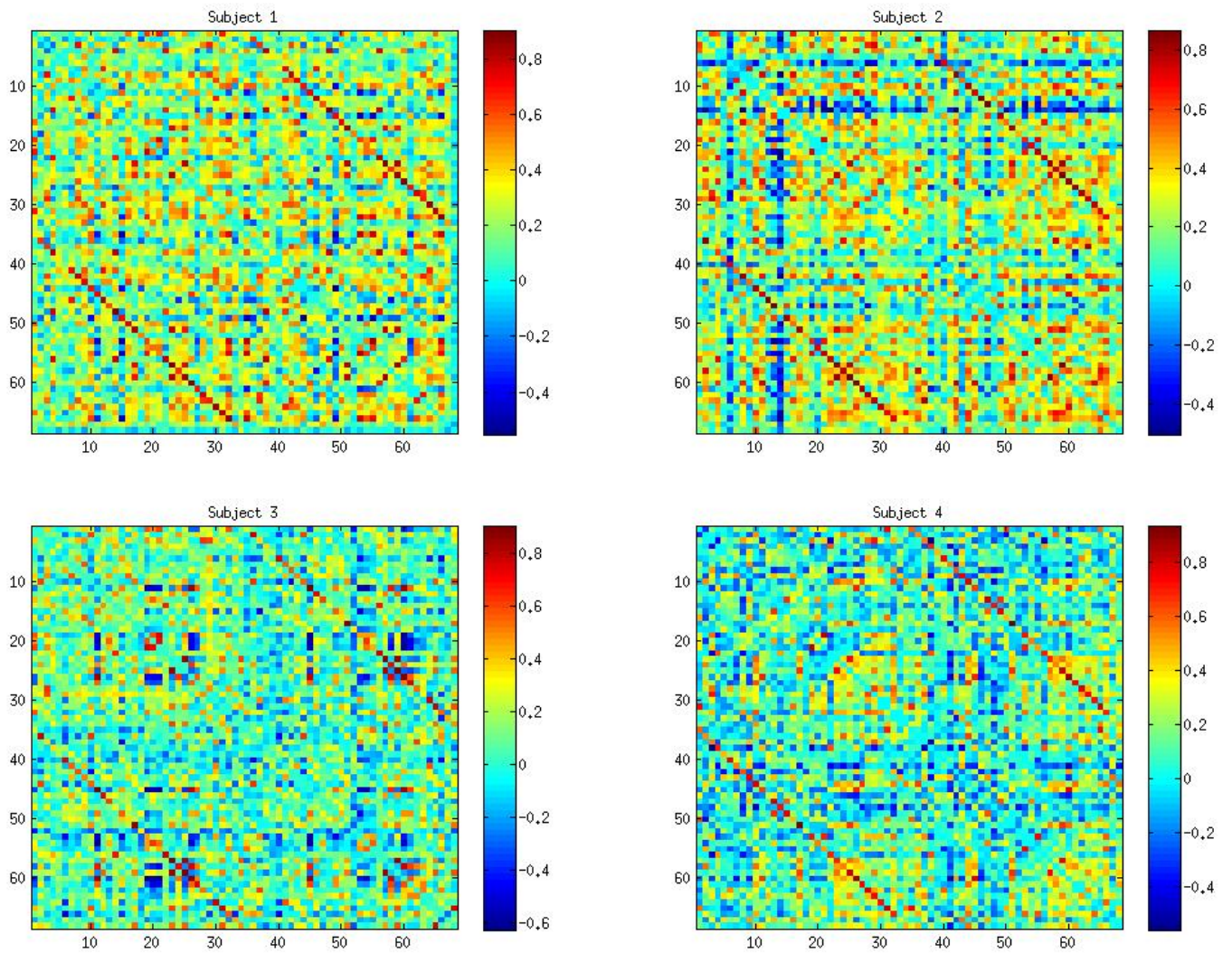


Figure B.1: Correlation coefficient map for subjects one to four.

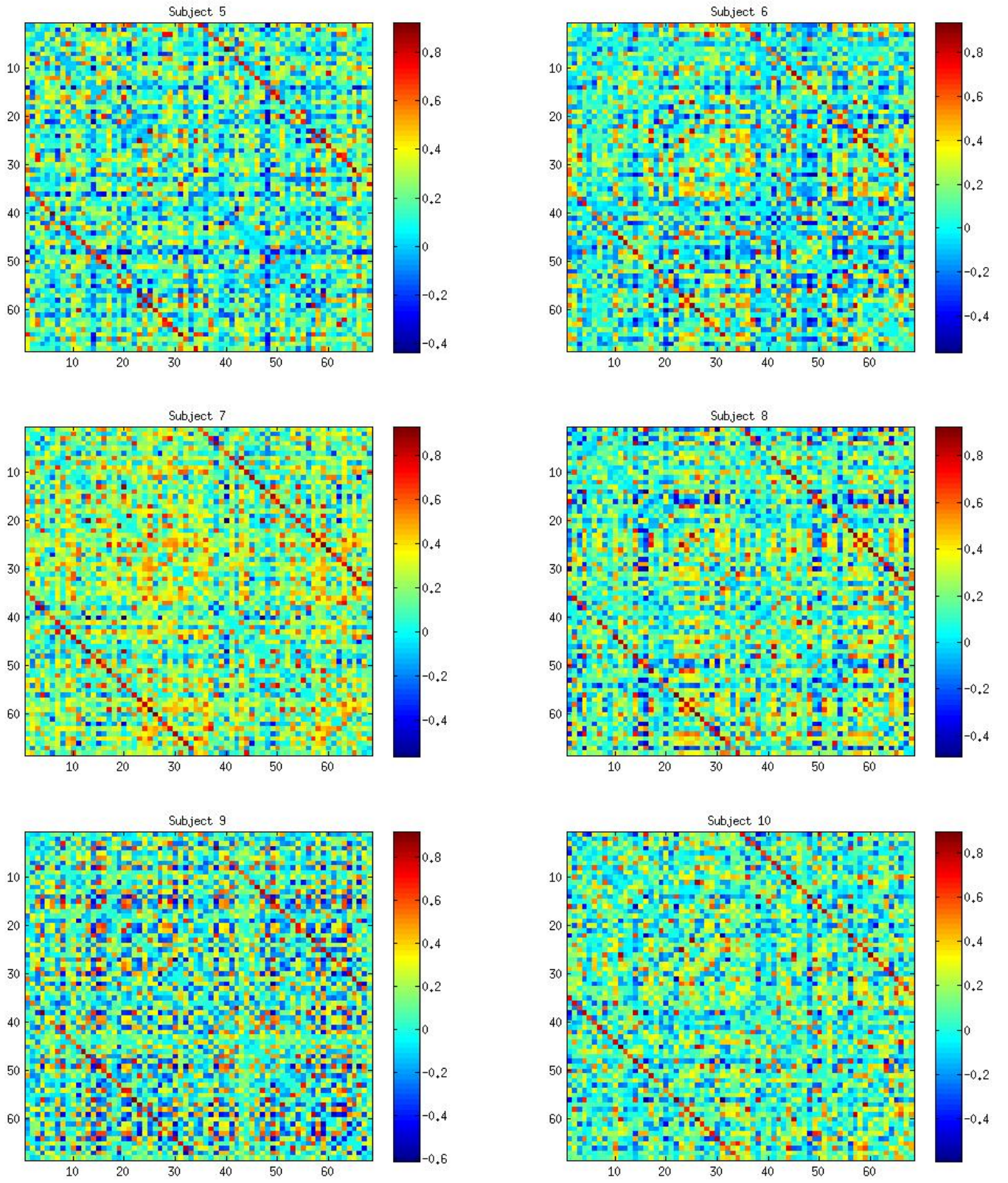


Figure B.2: Correlation coefficient map for subjects five to ten.

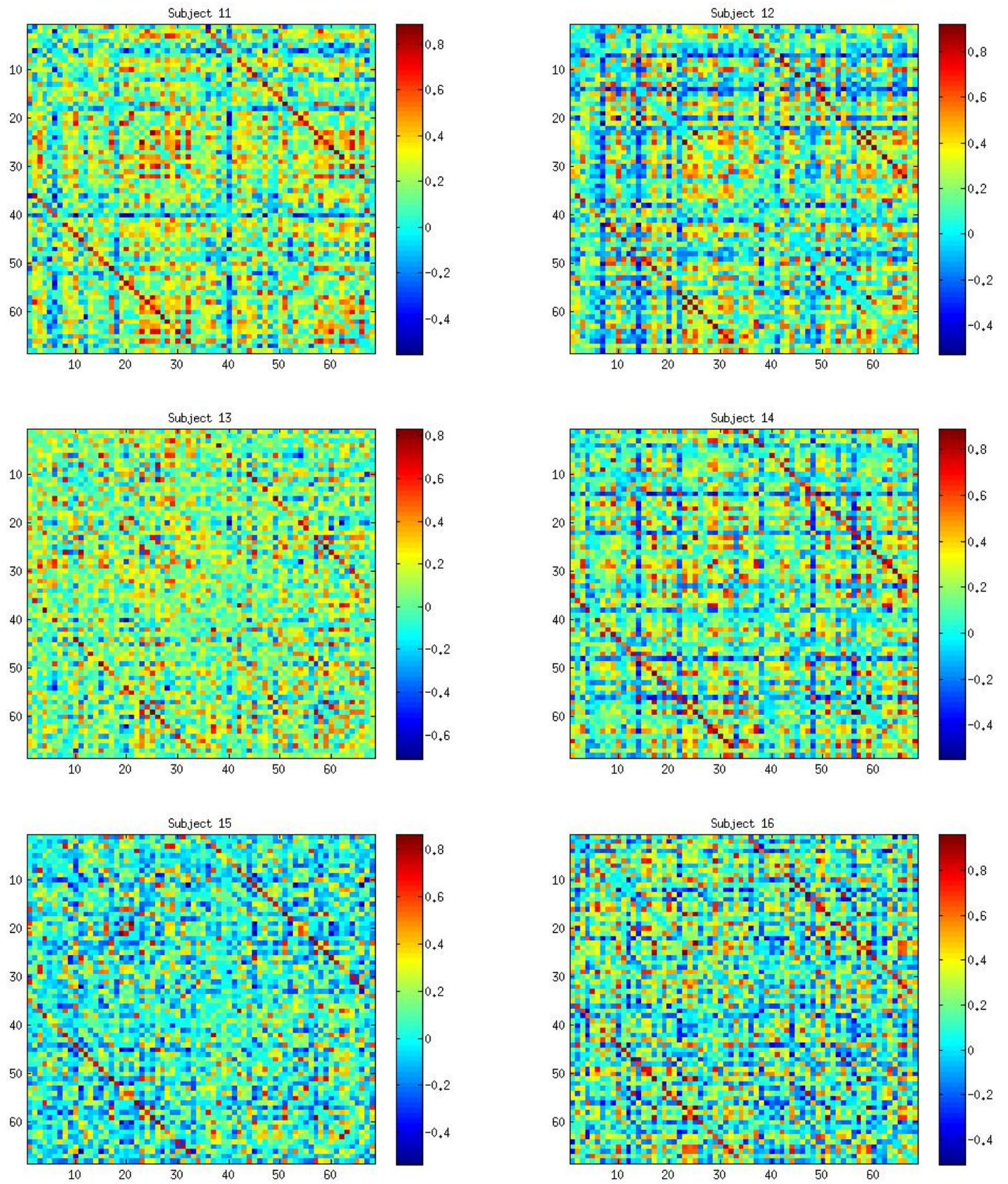


Figure B.3: Correlation coefficient map for subjects eleven to sixteen.

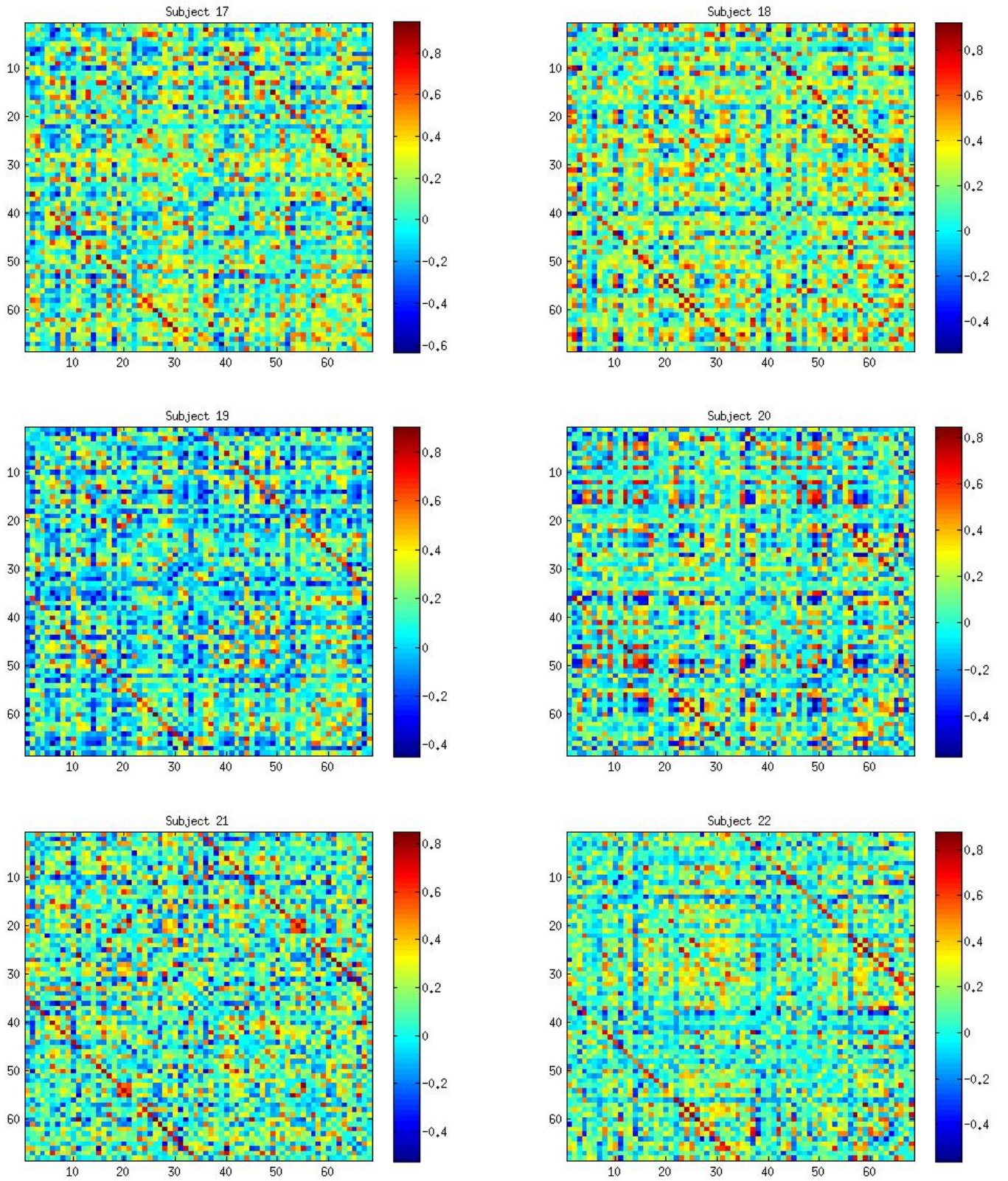


Figure B.4: Correlation coefficient map for subjects seventeen to twenty-two.

Appendix C

Statistical Analysis Plots

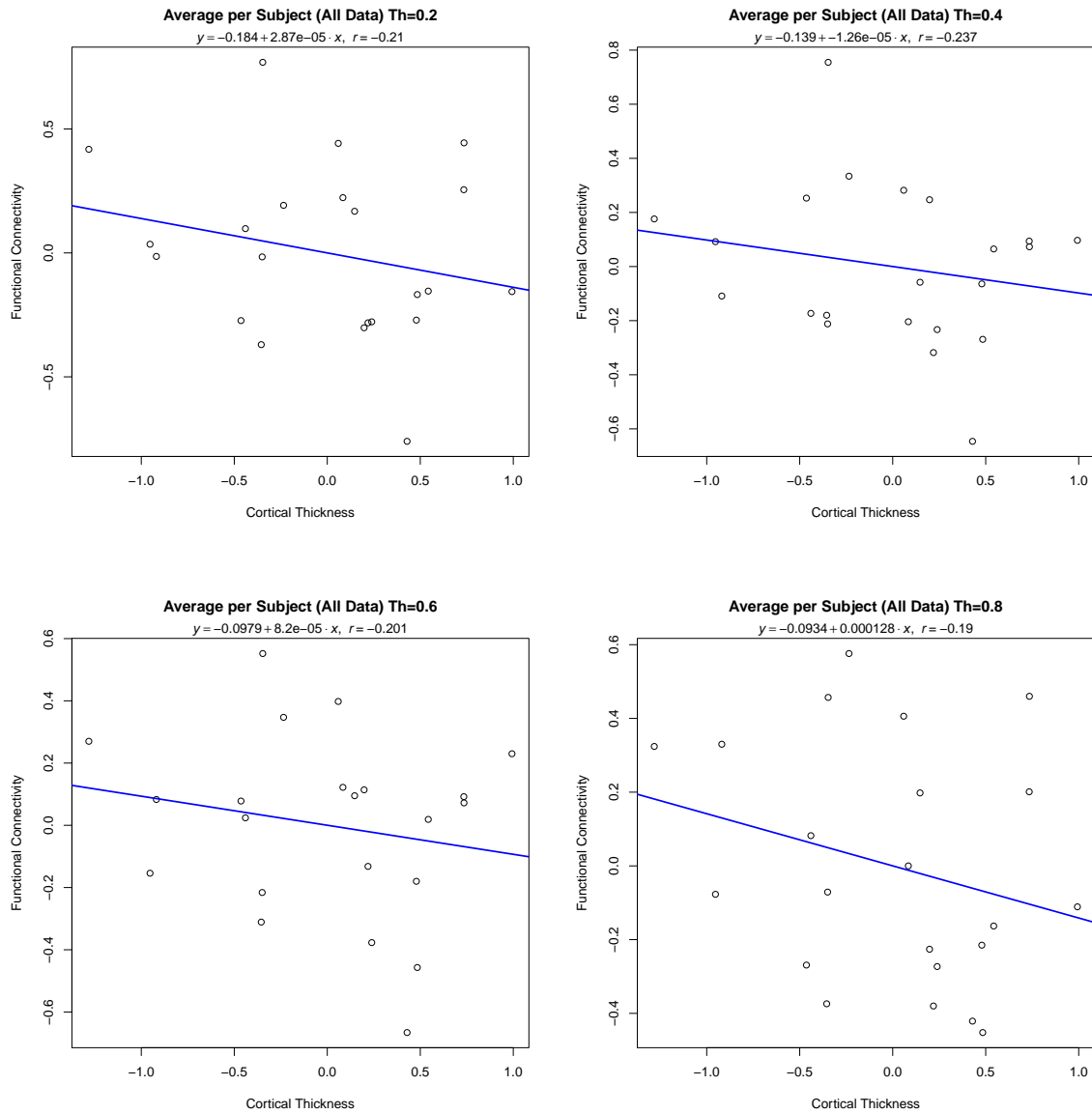


Figure C.1: Average correlation coefficients and cortical thickness by subject (using the whole data), applying a threshold of: (Top Left) 0.2; (Top Right) 0.4; (Bottom Left) 0.6; and (Bottom Right) 0.8.

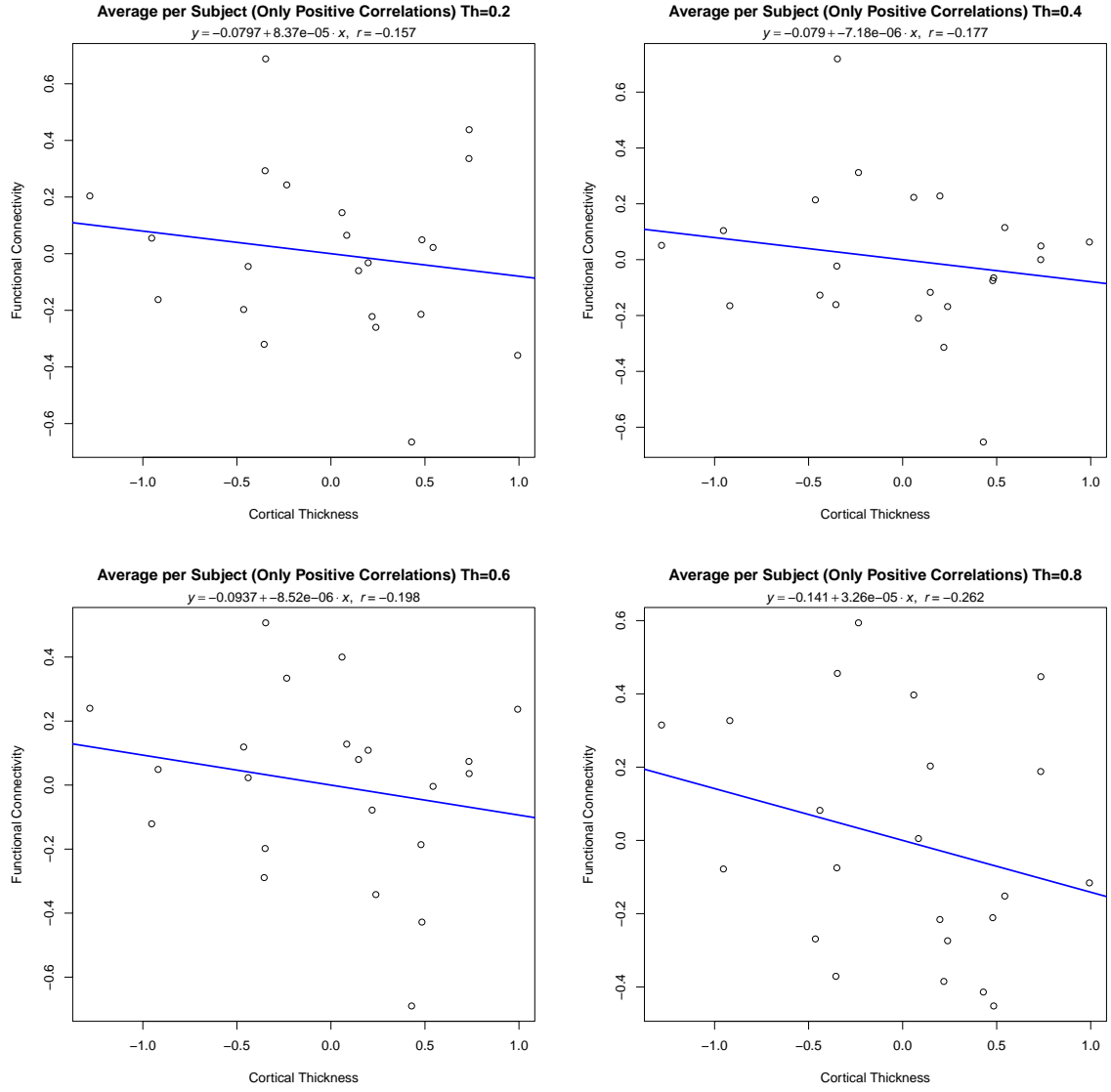


Figure C.2: Average correlation coefficients and cortical thickness by subject (using only the positive correlations), applying a threshold of: (Top Left) 0.2; (Top Right) 0.4; (Bottom Left) 0.6; and (Bottom Right) 0.8.

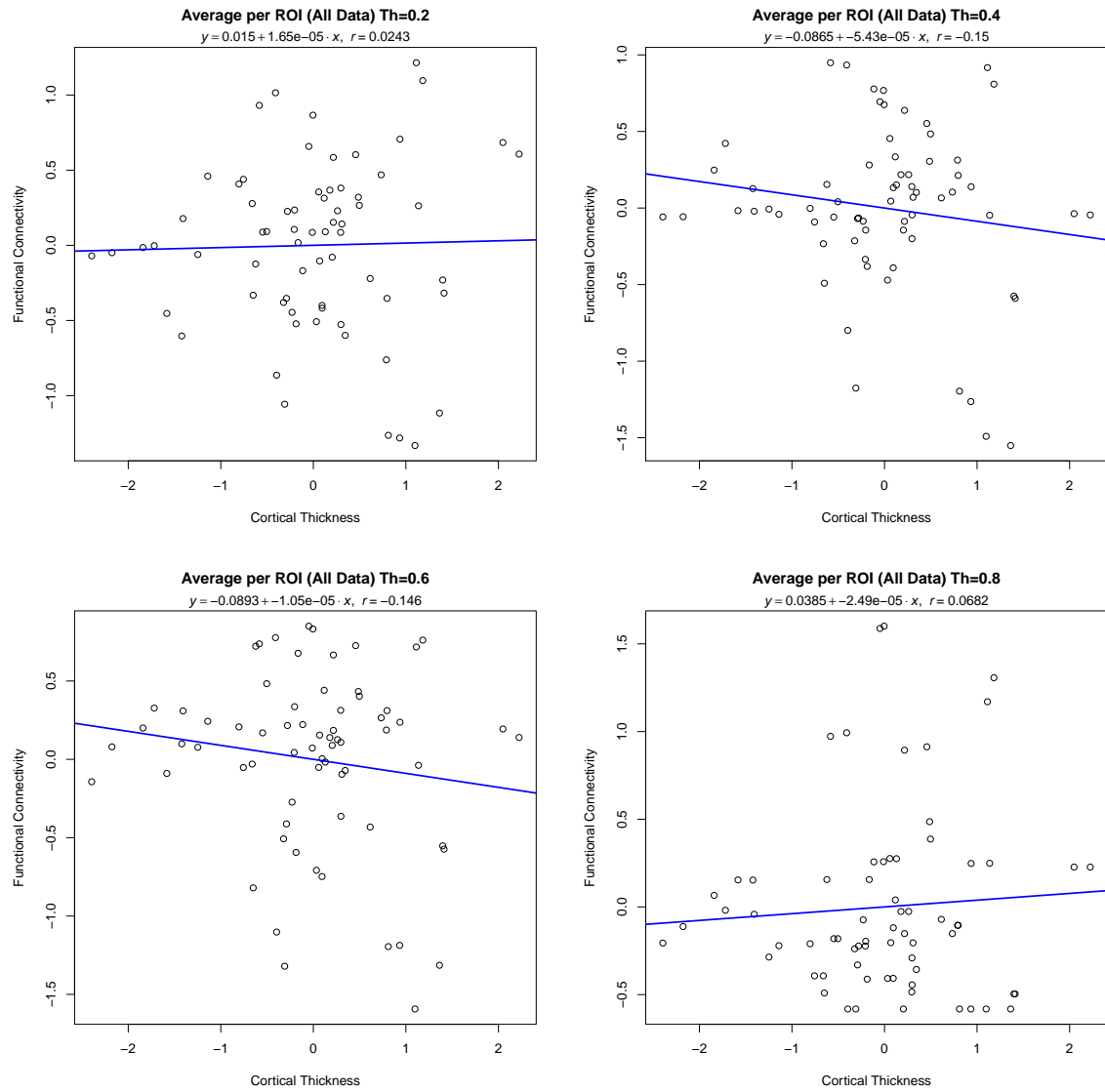


Figure C.3: Average correlation coefficients and cortical thickness by ROI (using the whole data), applying a threshold of: (Top Left) 0.2; (Top Right) 0.4; (Bottom Left) 0.6; and (Bottom Right) 0.8.

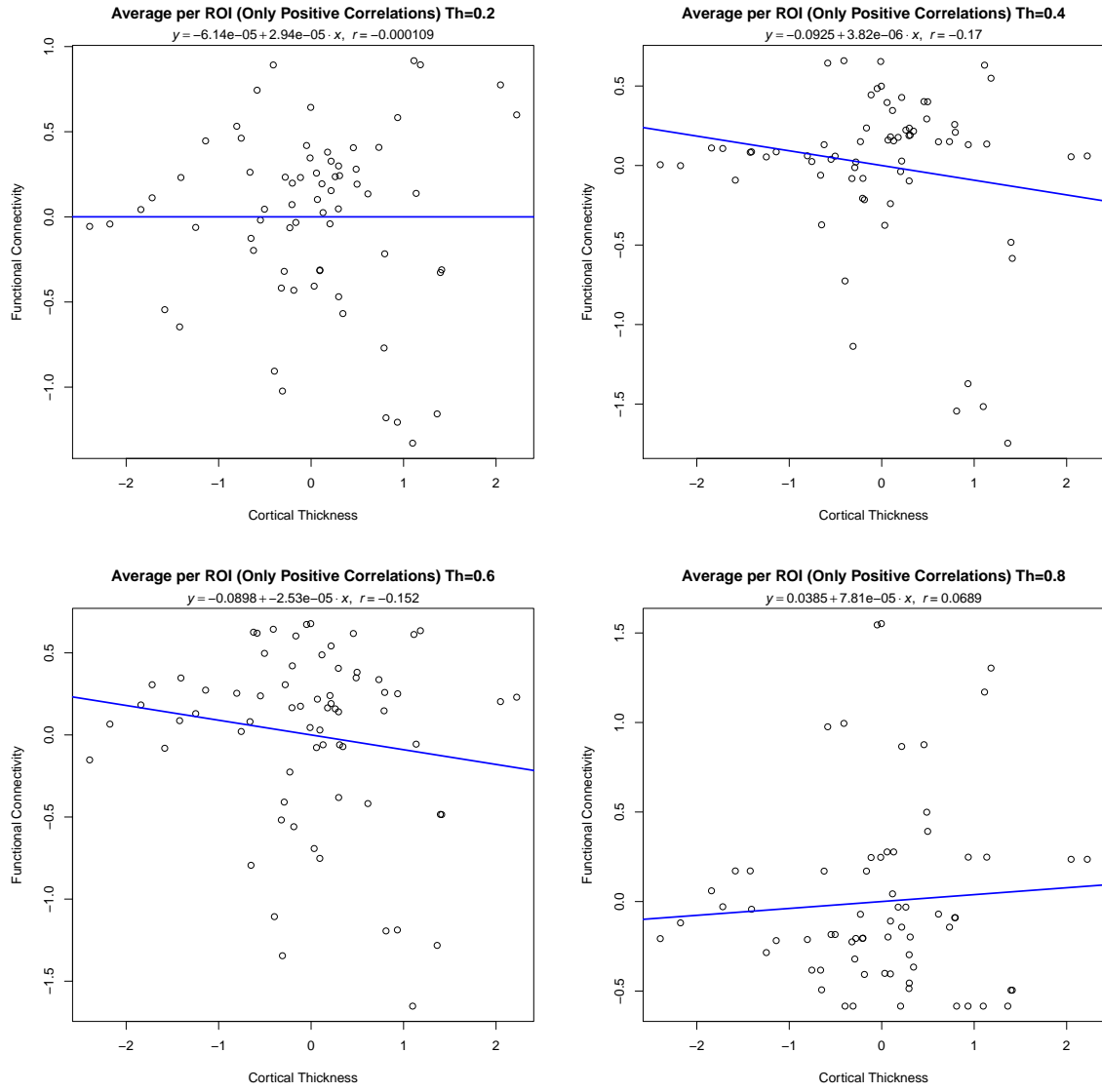


Figure C.4: Average correlation coefficients and cortical thickness by ROI (using only the positive correlations), applying a threshold of: (Top Left) 0.2; (Top Right) 0.4; (Bottom Left) 0.6; and (Bottom Right) 0.8.